Overview of ARIES-CS In-Vessel Components: Integration of Nuclear, Economic, and Safety Constraints in Compact Stellarator Design

L. El-Guebaly, P. Wilson, D. Henderson, M. Sawan, G. Sviatoslavsky, T. Tautges, R. Slaybaugh, B. Kiedrowski, A. Ibrahim, C. Martin, R. Raffray, S. Malang, J. Lyon, L.P. Ku, X. Wang, L. Bromberg, B. Merrill, L. Waganer, F. Najmabadi and the ARIES-CS Team

April 2007

UWFDM-1322

FUSION TECHNOLOGY INSTITUTE

UNIVERSITY OF WISCONSIN

MADISON WISCONSIN

Overview of ARIES-CS In-Vessel Components: Integration of Nuclear, Economic, and Safety Constraints in Compact Stellarator Design

L. El-Guebaly[1], P. Wilson[1], D. Henderson[1], M. Sawan[1], G. Sviatoslavsky[1], T. Tautges[2], R. Slaybaugh[1],

B. Kiedrowski[1], A. Ibrahim[1], C. Martin[1], R. Raffray[3], S. Malang[4], J. Lyon[5], L.P. Ku[6], X. Wang[3],

L. Bromberg[7], B. Merrill[8], L. Waganer[9], F. Najmabadi[3] and the ARIES-CS Team

April 2007

[1]Fusion Technology Institute
University of Wisconsin-Madison
1500 Engineering Drive
Madison, WI 53706, USA
http://fti.neep.wisc.edu

Phone: (608) 263-1623
Fax: (608) 263-4499
elguebaly@engr.wisc.edu

[2]Argonne National Laboratory, 9700 S. Cass Ave., Argonne, IL 60439, USA
[3]University of California, San Diego, 9500 Gilman Drive, La Jolla, CA 90093, USA
[4]Consultant, Fliederweg 3, D 76351 Linkenheim-Hochstetten, Germany
[5]Oak Ridge National Laboratory, Oak Ridge, TN 37831, USA
[6]Princeton Plasma Physics Laboratory, Princeton, NJ 08543, USA
[7]MIT Plasma Science and Fusion Center, Cambridge, MA 02139, USA
[8]Idaho National Laboratory, Idaho Falls, ID 83415, USA
[9]The Boeing Company, St. Louis, MO 63166, USA

UWFDM-1322

ABSTRACT

Within the ARIES-CS project, design activities have focused on developing a compact device that enhances the attractiveness of the stellarator as a power plant. The objectives of this paper are to review the nuclear elements that received considerable attention during the design process and provide a perspective on their successful integration into the final design. Among these elements are the radial build definition, the well-optimized in-vessel components that satisfy the ARIES top-level requirements, the carefully selected nuclear and engineering parameters to produce an economic optimum, the modeling – for the first time ever – of the highly complex stellarator geometry for the 3-D nuclear assessment, and the overarching safety and environmental constraints to deliver an attractive, reliable, and truly compact stellarator power plant.

I. INTRODUCTION

In recent years, the stellarator concept has emerged as a competitive source of fusion energy, offering a steady-state, non-disruptive operation. The most recent development of *compact* stellarators has led to the construction of the National Compact Stellarator Experiment (NCSX)[1] at the Princeton Plasma Physics Laboratory and the 3 year power plant study of ARIES-CS.[2] During the ARIES-CS design process, the principle of compactness drove the physics,[3] engineering, and economics.[4] The three design disciplines proceeded interactively and the systems code determined the reference parameters. The code[4] varied the physics and engineering parameters, subject to pre-assigned physics and technology limits, to produce an economic optimum. Basically, the ARIES-CS study aimed at reducing the stellarator size by:

- Developing a compact configuration with low aspect ratio (~ 4.5) and combination of advanced physics and technology.
- Optimizing the minimum plasma-coil distance (Δ_{min}) through rigorous nuclear assessment as Δ_{min} significantly impacts the overall size and cost.

An integral approach considering the design configuration, materials choice, design requirements, and component optimization was deemed necessary during the ARIES-CS design process. Based on lessons learned from previous ARIES studies, special care was taken in selecting the materials so that even in the unlikely accidental events, any environmental or release effect would be minimal or nonexistent. The collective impact of materials on the activation, safety, and waste management characteristics has done much to shape the design development during the three-year period of the study. As such, the nuclear analyses (neutronics, shielding, and activation) have been a fundamental element of the ARIES-CS study and have received considerable attention. Out of numerous nuclear-related questions, we identified the following top 5 sets of questions based on how fundamental to the stellarator concept they are and how much of an impact their solutions will have on the overall design:

1. How do the neutron wall loading (NWL) and radiation heating vary poloidally and toroidally? Where do they peak? Do the peaks occur at the same blanket module? What is the peak to average NWL ratio?
2. How compact can the design be? How far can we push Δ_{min}? Can the design tolerate a non-breeding blanket at Δ_{min}? What other components can be excluded at Δ_{min} to reduce its size? What is the impact of a truly compact Δ_{min} on the overall tritium breeding, machine size, and economics? Would a design with uniform blanket/shield everywhere be equally attractive?

3. What role does the overall tritium breeding ratio (TBR) play in defining the machine average major radius?
4. How can the complex stellarator configuration be modeled for the three-dimensional (3-D) nuclear analysis without geometrical approximations? Can the actual source strength be represented in real 3-D space?
5. Does a solution exist for the large radwaste volume generated by stellarators? How can the radwaste volume be minimized by design? Can the geological disposal option be avoided and replaced by recycling/clearance?

Stellarators promise disruption-free, steady-state operation with reduced recirculating power due to the absence of current-drive requirements. However, such advantages could be offset by the challenging engineering issues. Stellarators are quite complex machines. In ARIES-CS, the FW and surrounding in-vessel components conform to the plasma, as shown in Fig. 1, and deviate from the uniform toroidal shape in order to achieve compactness. Within each field period that covers 120 degrees toroidally, the configuration changes from a bean-shape at 0^{o} to a D-shape at 60^{o}, then back to a bean-shape at 120^{o}, continually switching the surfaces from convex to concave over a toroidal length of ~17 m. Figure 2 displays nine cross sections over a half field period showing the plasma boundary and the mid-coil filament. This means the FW and in-vessel component shapes vary toroidally and poloidally, representing a challenging 3-D modeling problem. In each field period, there are four critical regions of Δ_{min} (at ~11^{o} and 33^{o} in Fig. 2) where the magnets move closer to the plasma, constraining the space between the plasma edge and mid-coil. Δ_{min} should accommodate the scrapeoff layer (SOL), FW, blanket, shield, vacuum vessel, assembly gaps, coils case, and half of the winding pack. The penalty associated with increasing Δ_{min} by 10 cm is ~60 cm in the major radius and ~1 mill/kWh in the cost of electricity.[7] Being the most influential parameter for the stellarator's size and cost, its optimization was crucial to the overall design. An innovative approach was developed to downsize the blanket at Δ_{min} and utilize a highly efficient WC-based shield. This approach placed a premium on the full blanket to supply the majority of the tritium needed for plasma operation.

Modeling ARIES-CS for the 3-D nuclear analysis was a challenging engineering task. A novel approach based on coupling the CAD model with the MCNPX Monte Carlo code was developed to model, for the first time ever, the complex stellarator geometry for nuclear assessments (Sections II and IV). Accommodating the breeding blanket and necessary shield to protect the superconducting magnet at Δ_{min} represented another challenging task. Utilizing a non-uniform blanket combined with a highly efficient WC shield in this highly constrained region helped reduce the machine size and cost (Sections II, III, and IV). As stellarators generate more radwaste than tokamaks, managing ARIES-CS active materials

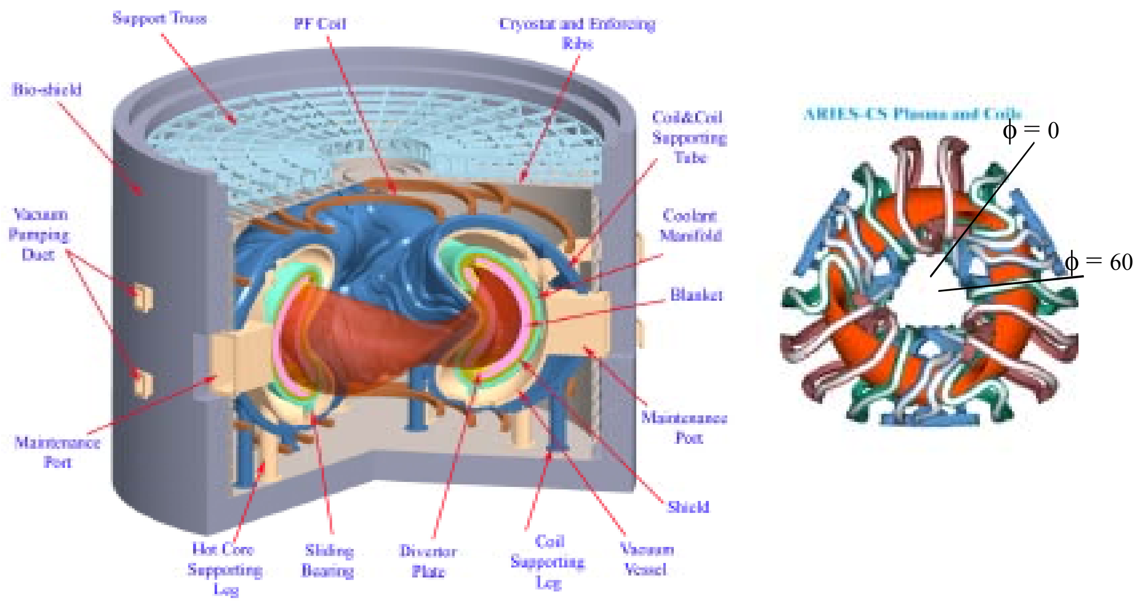

Fig. 1. Isometric view of ARIES-CS 3-FP configuration.

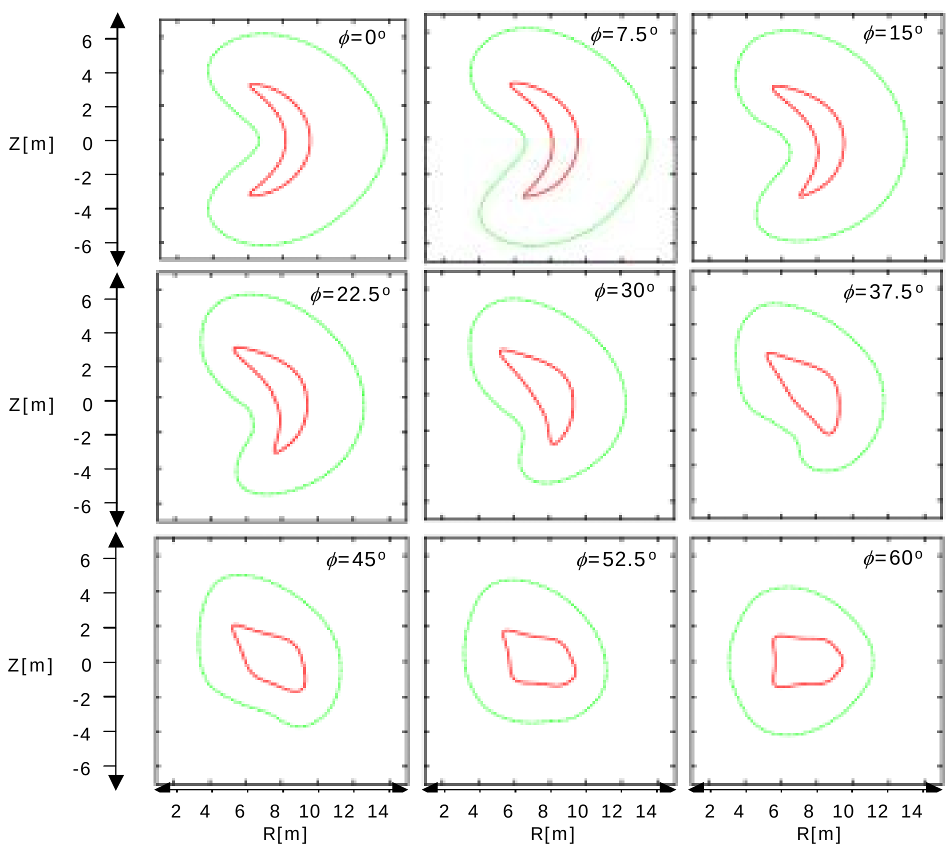

Fig. 2. Nine plasma and midcoil cross sections covering one half field period.

during operation and after plant decommissioning was essential for the environmental attractiveness of the machine (Section VI). Several additional nuclear-related tasks received considerable attention during the ARIES-CS design process. These included the radial build definition, the well-optimized in-vessel components that satisfied the top-level requirements, the streaming of neutrons through the helium access tubes and pipes, the carefully selected nuclear and engineering parameters to produce an economic optimum, and the overarching safety constraints to deliver a safe and reliable power plant. This paper describes the successful integration of the nuclear design elements into the reference three field period (FP) ARIES-CS design. Previous supporting analyses performed for interim designs are included in References 4-6.

At the outset, the design process itself took into consideration the fabricability, constructability, operability, and maintainability of the machine.[8,9] To ensure the top-level requirements[10] are fully incorporated, a subset of nuclear-related requirements was established for the ARIES-CS design, as summarized in Table I. As will be discussed shortly, a tritium-breeding ratio (TBR) of 1.1 assures tritium self-sufficiency. A flexible blanket design could adjust the net TBR after operation in case of overbreeding or underbreeding. The life-limiting criteria for the structural components and magnets are key factors to accurately determine their lifetimes. We adopted high radiation limits in concert with similar ground rules considered in the past for advanced ARIES designs.[11-13] The nuclear heat leakage from the power producing components to the surroundings must remain below 1% to enhance the power balance. If there is a need to cut and reweld the manifolds and VV, the helium production level should not exceed 1 appm at any time during operation. No high-level waste should be produced to avoid deep geological burial. The disposal option could be replaced with more environmentally attractive scenarios, such as recycling and clearance.

The following sections document the detailed analyses and results for the LiPb/He/FS reference design and to a lesser extent for the LiPb/SiC backup system. Throughout this study, the neutronics and shielding assessments were evaluated with the MCNPX 3-D Monte Carlo code[14] and its IAEA FENDL-2 data library and the DANTSYS discrete ordinates transport code[15] with the IAEA FENDL-2 175 neutron 42-gamma group coupled cross-section library.[16] The activation results were computed with the ALARA pulsed activation code[17] and the IAEA FENDL-2 175 neutron group transmutation cross-section library.[16]

Table I
ARIES-CS Design Requirements and Radiation Limits

Overall TBR (for T self-sufficiency)	1.1	
Damage to Structure (for structural integrity)	200 3%	dpa - advanced FS burnup for SiC
Helium Production @ Manifolds and VV (for reweldability of FS)	1	He appm
Nuclear Heat Leakage	< 1%	
S/C Magnet (@ 4 K):		
Peak fast n fluence to Nb_3Sn (E_n > 0.1 MeV)	10^{19}	n/cm^2
Peak nuclear heating	2	mW/cm^3
Peak dpa to Cu stabilizer	$6x10^{-3}$	dpa
Peak dose to electric insulator	10^{11}	rads
Plant Lifetime	40	FPY
Availability	85%	
Operational dose to workers and public	< 2.5	mrem/h
LLW level	Class A or C	
Radwaste minimization	Recycle and/or clear	

* Acronyms: TBR for tritium breeding ratio, dpa for displacement per atom, appm for atom part per million, LLW for low-level waste, FPY for full power year.

II. NEUTRON WALL LOADING AND RADIATION FLUX PROFILES

To take full advantage of the three-dimensional (3-D) neutron transport modeling capability enabled by the CAD-based MCNPX-CGM tool,[18] it is necessary to generate the neutron source with a full representation of the 3-D variations in the source intensity. Traditional methods of defining a neutron source for Monte Carlo analysis of a fusion system assume varying degrees of symmetry. For example, for most tokomak systems, the neutron source is defined on a 2-D R-Z cylindrical mesh with the assumption of cylindrical symmetry. For ARIES-CS, not only is there no toroidal symmetry, but the complex mathematical source representation does not lend itself to a standard R-Z-Θ cylindrical mesh either. A new strategy for representing the 3-D variations in neutron source strength (i.e. fusion power) for use in Monte Carlo transport calculations was developed with three steps:

1. A regular, uniform mesh is generated in flux coordinate space, (Θ,Φ,s), where Θ is the toroidal angle, Φ is the poloidal angle, and s is the flux surface number. The Fourier description of the plasma flux surfaces can then be used to transform these points to a cylindrical coordinate system, (R,Z,Θ), in real space, which can then be transformed to a Cartesian coordinate system, (X,Y,Z). Care must be taken to properly account for the fact that the hexahedra (“hexes”) adjacent to the magnetic axis are degenerate, manifested as prisms rather than true hexes.
2. The flux surfaces represent iso-surfaces of constant plasma temperature and density, and therefore, constant fusion power and neutron source density. Therefore, as every point in the (X,Y,Z) mesh represents a point on a known flux surface, the neutron source density can be evaluated at each point and a hex-averaged source density can be determined. The relative probability that a source is born in a given hex is simply the product of the hex-averaged source density and the hex volume. A cumulative distribution function (CDF) over the entire set of hexes can be found from the normalized probabilities and provided to a Monte Carlo code for sampling. In particular, the mesh vertices and hex-CDF values are written to a file for use by the Monte Carlo code.
3. Within the Monte Carlo code, MCNPX-CGM in this case, finding the birth location of each source neutron begins by sampling the discrete CDF that represents the set of hex probabilities. Once the particular hex is known and its eight vertices have been identified (six vertices of hexes adjacent to the magnetic axis), the hex is sampled uniformly to determine a position, (X,Y,Z), within that hex.

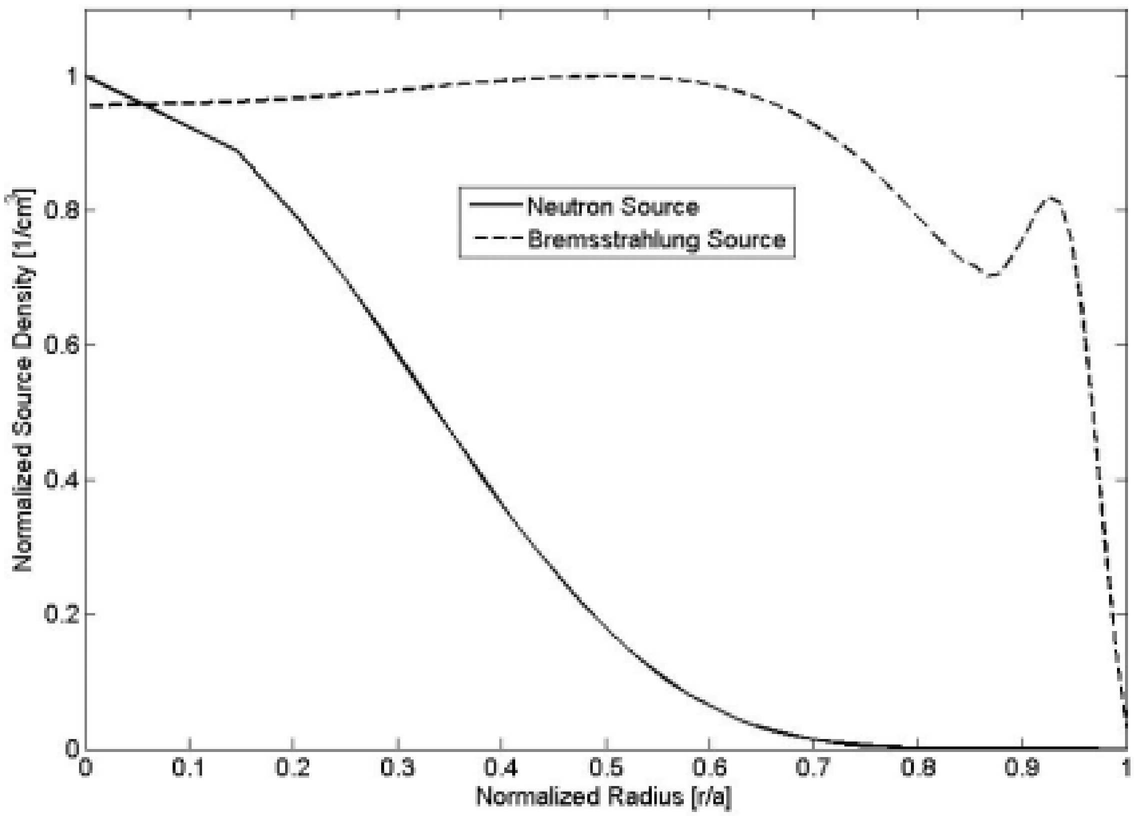

Fig. 3. Neutron and radiation heating sources.

This scheme has proven useful in modeling the ARIES-CS source distribution (see Fig. 3), but could form the basis for an improved coupling of the neutron source to the transport calculation for all magnetically confined fusion systems. Ongoing improvements are being incorporated to allow higher-order mesh spacing, source averaging, and sub-hex position sampling.

II.A. Neutron Wall Loading Distribution

As with all fusion systems, the neutron wall loading (NWL) is a valuable quantity to assess the scaling of neutron responses on local system components. Calculating the spatial variations of the NWL for the complex geometry of the ARIES-CS system requires advanced neutronics methods. The CAD-based MCNPX-CGM tool provides just such a capability.

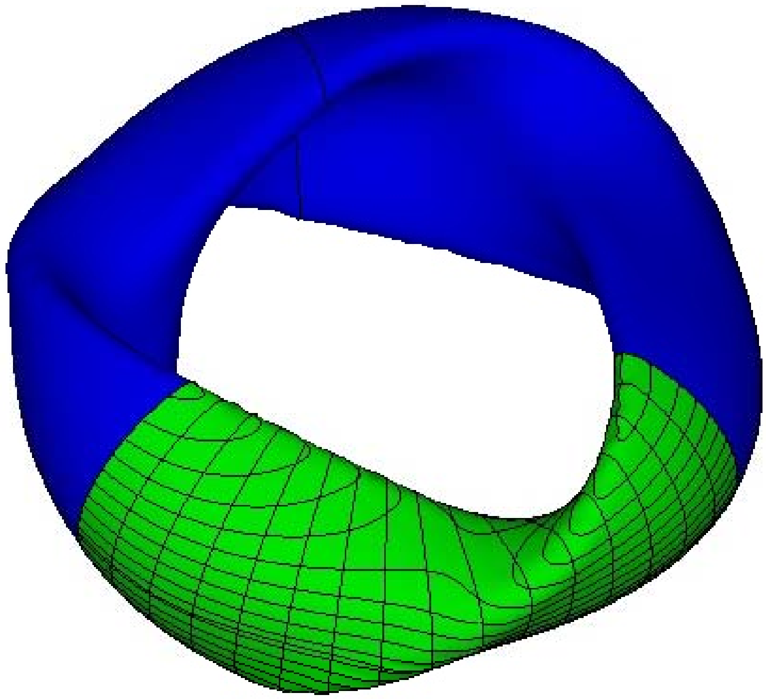

Fig. 4. Model of first wall for 5 cm scrap-off layer NWL calculation, showing segmentation of first wall over 120° of toroidal extent.

Using the Fourier description of the last closed magnetic surface (LCMS), a plasma surface was created using the CUBIT solid-modeling tool.[19] From this, two separate geometries were generated to represent different offsets between the plasma and first wall. In one case, a 5 cm scrape-off layer was modeled by creating a first wall surface with a 5 cm offset from the LCMS surface. In the other case, a 30 cm offset was used to model the regions of the first wall that would be moved further away from the plasma. As is the convention for NWL calculations, only the uncollided neutron current is measured at the first wall. To accommodate this, the space outside the first wall surface was defined to be a perfect absorber (zero importance in the vernacular of MCNPX).

For each geometry, one third of the toroidal extent of the first wall surface was segmented using CUBIT to allow for spatial resolution of the NWL calculation. In the toroidal direction, a spacing of 7.5° gave 16 segments, while a spacing of 40 cm in the axial (Z) direction gave a varying number of axial segments depending on the toroidal position and magnitude

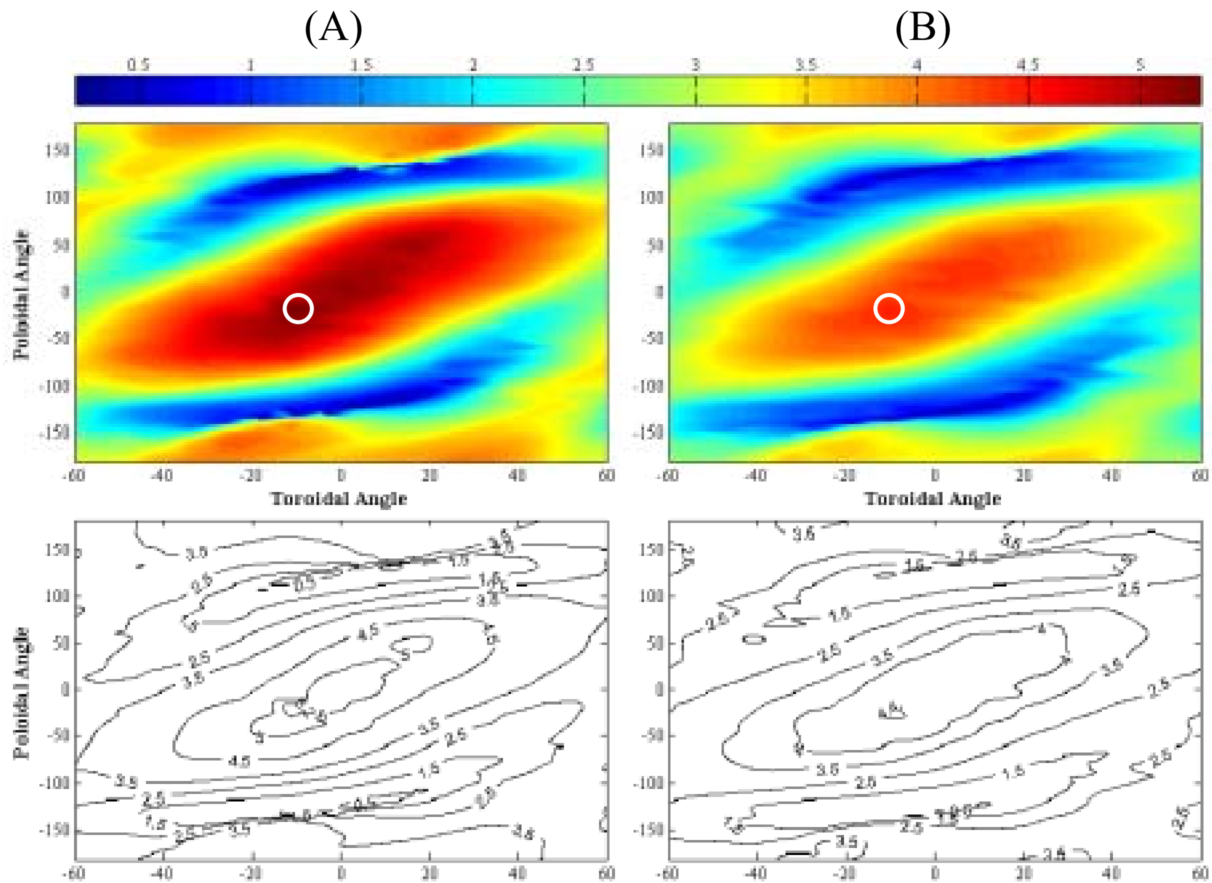

Fig. 5. Contour maps of the NWL [in MW/m^2] for the 5 cm (A) and 30 cm (B) scrape-off layer geometries. The approximate location of the peak is indicated with circles. The toroidal angle is measured from the beginning of the field period while the poloidal angle is measured from the outboard midplane at the level of the magnetic axis.

of the first wall offset (see Fig. 4). This resulted in 352 segments for the 5 cm SOL case and 472 segments for the 30 cm SOL case.

The uncollided neutron current through each surface was tallied using MCNPX-CGM (F1 tally) and divided by the surface area for each segment, as reported by CUBIT, normalized to the total fusion power of the system, and reported at the midpoint of each segment. Post-processing, performed with MATLAB, mapped those results onto a coordinate system based on the toroidal and poloidal angles, (Θ,Φ), relative to the magnetic axis. The results were interpolated onto a 600 x 600 grid, uniform in Θ=[-60°,60°] and Φ=[-180°,180°], to generate two dimensional NWL maps and extract poloidal variations in NWL with poloidal angle at specific toroidal angles.

The NWL from the 3-D neutron source was analyzed for both cases (5 cm and 30 cm scrape-off layers), and contour maps are shown in Fig. 5 for a fusion power of 2355 MW. Both exhibit the same general distribution, with similar locations of the maximum and minimum NWL values. In addition to reducing the peak NWL from 5.3 to 4.4 MW/m^2, the minimum NWL increases from 0.32 to 0.42 MW/m^2. In both cases, the peak is identified near the midplane (=-18° or -25°) at a toroidal angle of -11°. However, given the statistical error of the results, it is more important to recognize the large area within 10% of the peak NWL, extending approximately 60° (-30° to 30°) in the toroidal direction and 140° (-70° to 70°) in the poloidal direction. The minimum neutron wall loading occurs near the divertor region at approximately ±120° in the poloidal direction and extending approximately 20° (-10° to 10°) in the toroidal direction. Figure 6 shows the detailed poloidal distributions of the NWL at various toroidal angles. In each case, the poloidal distribution at the location of the peak NWL (-11°) is included. Notice that the maximum NWL at a toroidal angle of 0° is close to the overall maximum, consistent with the earlier observation that a substantial wall area is exposed to a NWL near the maximum.

The reference configuration selected for ARIES-CS deviates somewhat from the standard practice of uniform scrape-off layers (SOL). It calls for 5 cm SOL everywhere, except at the divertor where the SOL expands to 30 cm to maintain the heat flux at the divertor surface within a tolerable level. The FW area, including the divertor, is ~730 m^2 and for 1885 MW neutron power, the average NWL amounts to 2.6 MW/m^2. This means the peak to average NWL ratio is approximately two. Of interest is the drop of this ratio with the plasma aspect ratio (defined as the average major radius divided by the average, circularized minor radius). Figure 7 displays the less steep variation for stellarators[20,21] compared to tokamaks.[12,13]

II.B. Radiative Heating Distribution

In addition to the NWL, the core radiation distribution on the first wall was calculated using the same methodology, but using the source profiles for the 354 MW Bremsstrahlung radiation being emitted by the plasma (refer to Fig. 3). Since this source distribution is much closer to a uniform distribution, the peak location moves to a toroidal angle of -34° at a poloidal angle of -17°. The maximum first wall heat flux due to core radiation is 0.68 MW/m^2 while the average value is 0.48 MW/m^2. Figure 8 shows that the region where the maximum heating from core radiation occurs is in a different location from the regions of maximum NWL. As with the NWL, Fig. 9 shows the poloidal distributions of the core radiative heating at a number of toroidal angles. The final design values for the first wall heat flux should also include other smaller edge radiation components, resulting in overall maximum and average first wall heat flux values of 0.76 and 0.57 MW/m^2, respectively.[7,22]

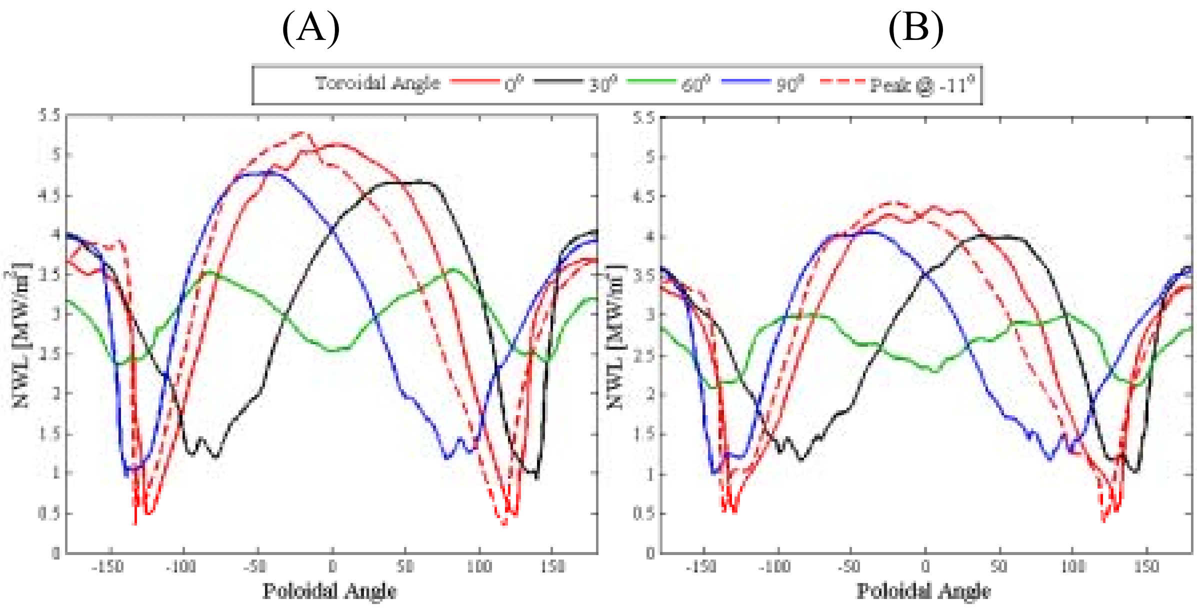

Fig. 6. Poloidal distributions of NWL at various toroidal angles, including the location of the peak NWL. (A) 5 cm scrape-off layer (B) 30 cm scrape-off layer. The poloidal angle is measured from the outboard midplane at the level of the magnetic axis.

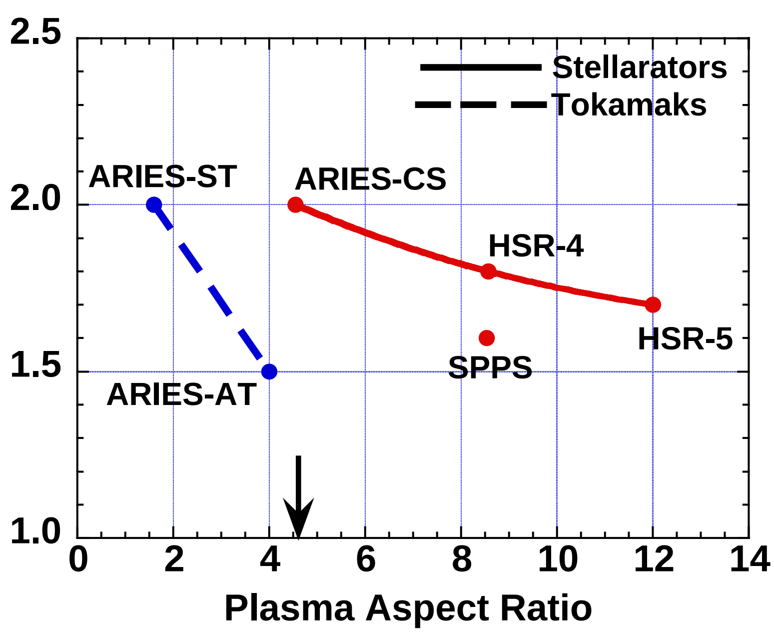

Fig. 7. Reduction of peak to average NWL ratio with stellarator plasma aspect ratio. The tokamak curve is shown for comparison.

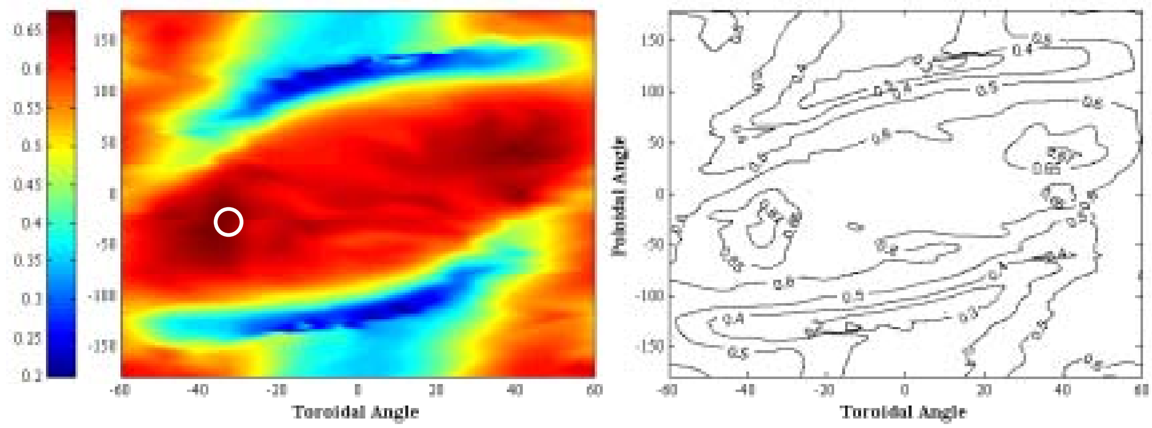

Fig. 8. Contour map of the core radiation on the first wall with a 5 cm scrape-off layer. The toroidal angle is measured from the beginning of the field period while the poloidal angle is measured from the outboard midplane at the level of the magnetic axis.

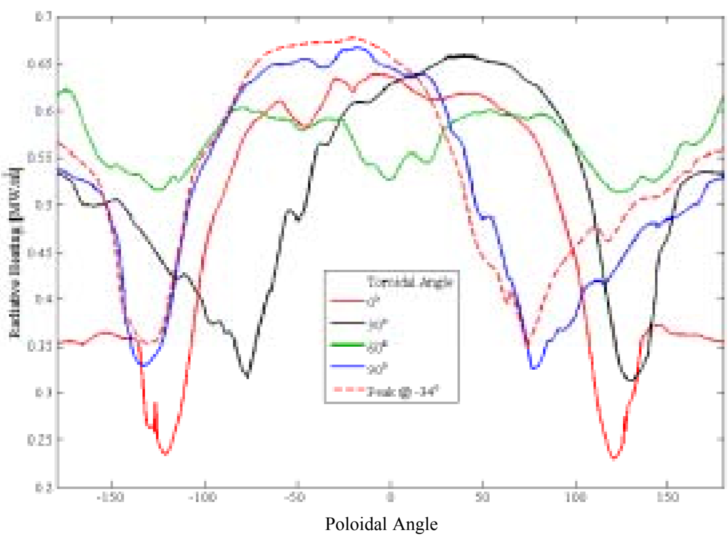

Fig. 9. Poloidal distribution of the core radiation, including the location of the peak heating. The poloidal angle is measured from the outboard midplane at the level of the magnetic axis.

III. RADIAL BUILD DEFINITION

The reference ARIES-CS design employs dual coolants (LiPb and He) to recover the heat from the power producing components (FW, blanket, shield, manifolds, and divertor). One of the advantages of using dual coolants is to provide redundancy in case of accident and to ultimately protect the design from off-normal scenarios, such as loss of either coolant or flow events. While the ferritic steel-based blanket[22] is based on the same concept developed earlier by the ARIES team for the ARIES-ST spherical tokamak,[12] and later considered as an ITER blanket testing module by many ITER parties, the unique blanket safety features were thoroughly examined and analyzed to provide assurance of their effectiveness.[23-25] A coolant with more efficient shielding performance (such as water) was employed for the vacuum vessel (VV) – a non-producing power component. Because of the high reliability of the VV cooling system, water can flow naturally, carrying the decay heat out of the in-vessel components during accidents, enhancing the safety features of the design.[23,24]

The compactness of the machine mandates that all components provide a shielding function. We started the nuclear assessment by defining the FW, blanket, and back wall parameters (thickness, composition, and Li enrichment). Next, the shield was designed to protect the welds of the manifolds and VV. Finally, the VV composition and dimension were optimized to essentially protect the superconducting magnets that operate at 4 K. All materials were carefully chosen to enhance the shielding performance and minimize the long-term environmental impact. We periodically checked and determined the key nuclear parameters with a series of 1-D and 3-D analyses[4,5,6] and the results were constantly reviewed for potential design modifications. All components have been sized for the maximum NWL and designed to provide adequate performance margins compared to requirements. The reference radial builds are shown schematically in Fig. 10 for two cross sections through the nominal, full blanket (designed for a peak NWL of 5.3 MW/m^2) and at Δ_{min} (designed for 3.3 MW/m^2 NWL – the maximum at the non-uniform blanket region). The FW, blanket, back wall, and divertor system are replaceable components, while all components outside the back wall are permanent with 40 FPY lifetime. Figure 11 demonstrates a toroidal cross section through the non-uniform blanket as envisioned for the transition region between Δ_{min} and the full blanket. Table II lists the compositions of all components while the alloying elements and impurities are given in Ref. 26.

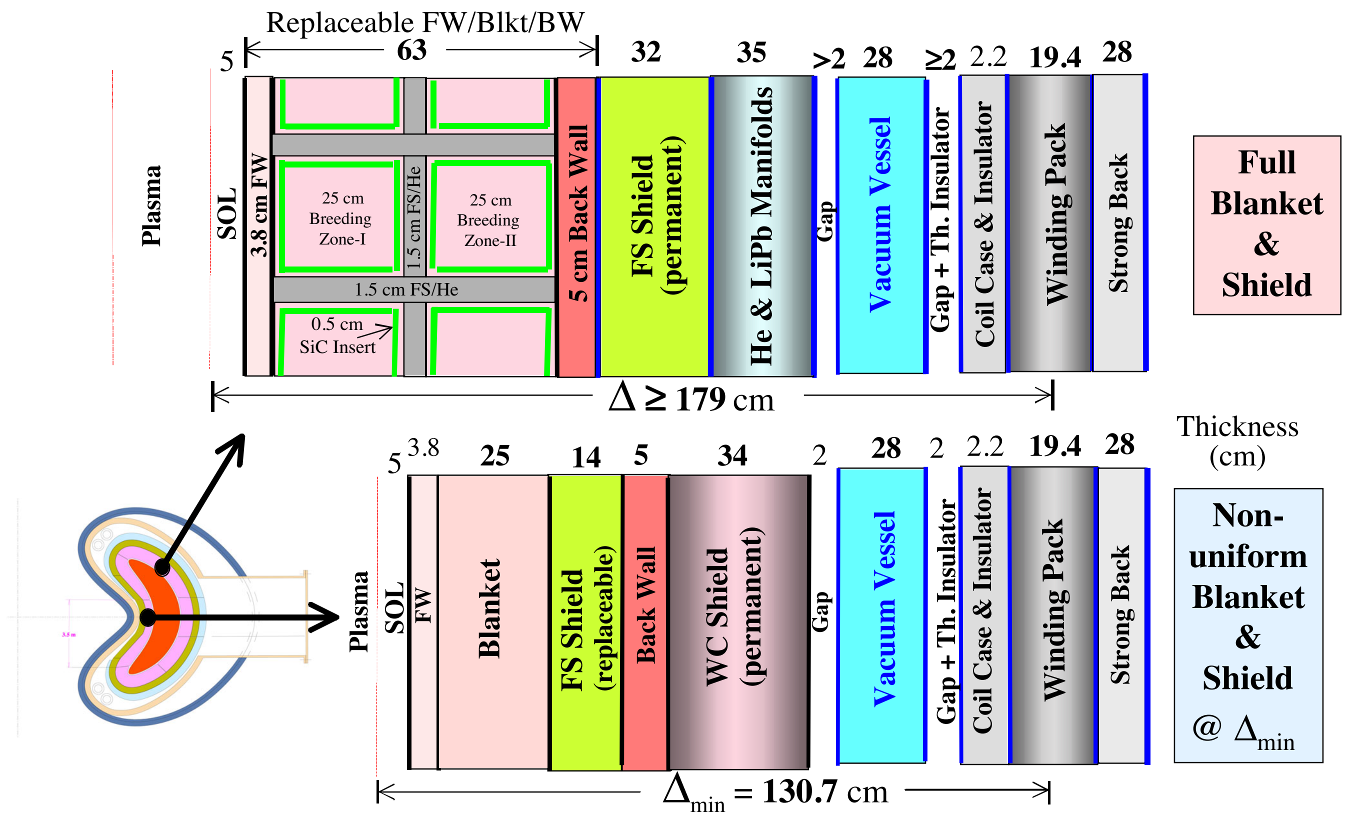

Fig. 10. Radial builds for the reference LiPb/He/FS blanket.

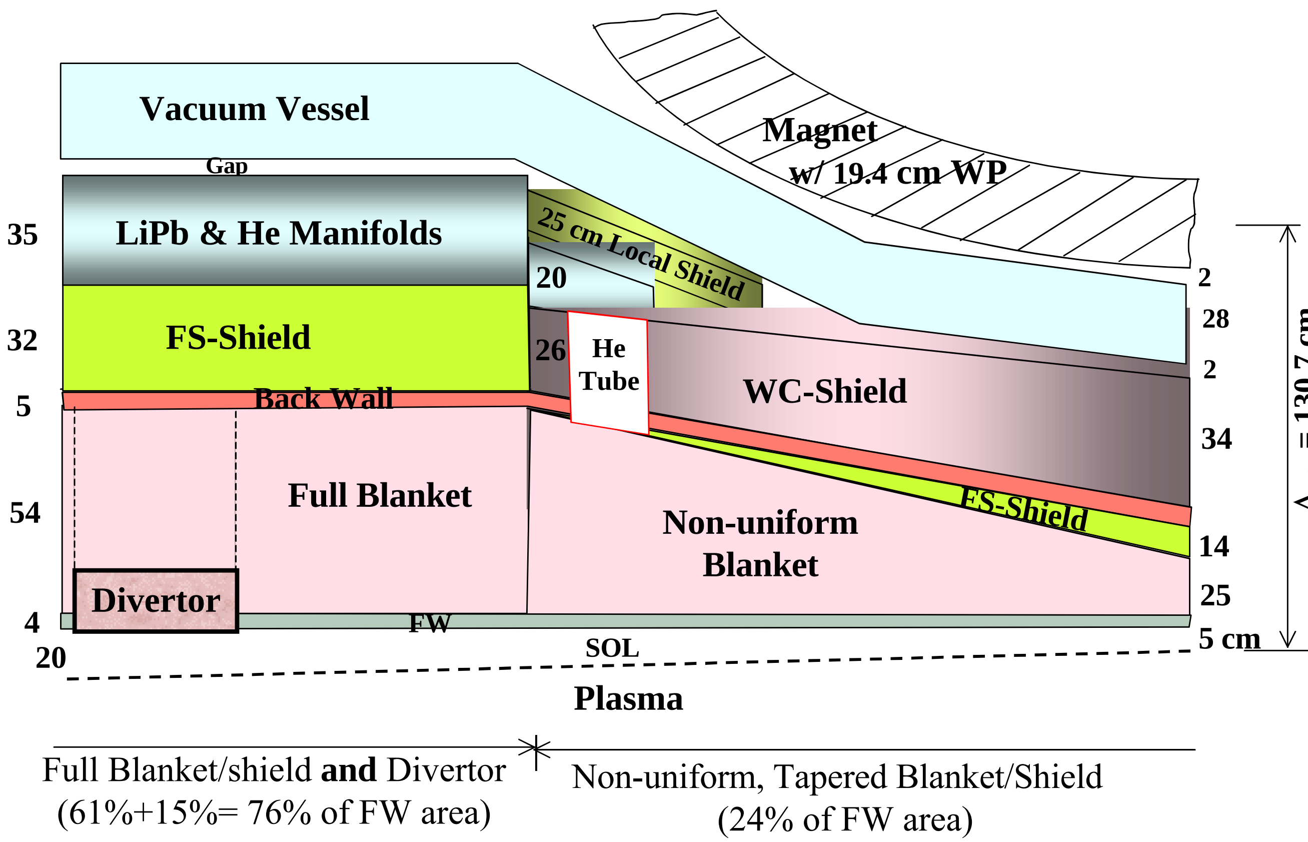

Fig. 11. Toroidal cross section through uniform and non-uniform blankets, showing the He feeding tube for the latter.

Table II

Compositions of ARIES-CS Components

	LiPb*/He/FS	**LiPb*/SiC**
FW	34% FS Structure 66% He Coolant	--- (integrated with blanket)
Divertor System	32.6% FS Structure 4.0% W 63.4% He Coolant	33% SiC/SiC Structure 4% W 63% LiPb (< 90% enriched Li)
Full Blanket	79% LiPb (70% enriched Li) 7% SiC Inserts 6% FS Structure 8% He Coolant	21% SiC/SiC Structure 79% LiPb (< 90% enriched Li)
Back Wall	80% FS Structure 20% He Coolant	---
FS or SiC Shield	15% FS Structure 10% He Coolant 75% Borated Steel Filler	15% SiC/SiC Structure 10% LiPb Coolant 75% Borated Steel Filler
WC Shield	15% FS Structure 10% He Coolant 75% WC Filler	---
Manifolds	52.0% FS Structure 22.7% LiPb (≤ 90% enriched Li) 24.0% He Coolant 1.3% SiC Inserts	---
Vacuum Vessel	28% FS Structure 49% Water 23% Borated Steel Filler	
Inner Coil Case, Strong Back, and Intercoil Structure	95% JK2LB Structure 5% LHe Coolant	
Winding Pack	18.5% JK2LB Structure 48.2% Cu 12.8% Nb_3Sn 10.0% Insulator 10.5% LHe Coolant	
Cryostat	100% 304-SS Structure	
Bioshield	85% Concrete 10% Mild Steel 5% He coolant	

* 17 at% Li and 83 at% Pb.

As will be discussed later in Section IV, two blanket and shield concepts received considerable attention during the ARIES-CS study: the reference, near-term LiPb/He/FS system and the backup, more advanced LiPb/SiC system. Due to the absence of He coolant, the LiPb/SiC system offers a more compact nominal radial build, as illustrated in Fig. 12. Note that the radial standoff at Δ_{min} was kept fixed at 1.3 m to keep the major radius at 7.75 m in order to meet the breeding requirement and FW heat load limit. Filling the 1.3 m space with blanket and shielding materials provides more protection for the VV and magnet than actually needed and suggests borated FS (B-FS) filler for the shield, instead of WC.

The main deliverables are summarized in Table III and the following Sections (IV and V) provide the details of the supporting analyses. It should be mentioned that the 50 cm reduction resulting from the compact radial build at Δ_{min} is estimated to save 25-30% in the major radius and cost of electricity,[7] which is significant. The benefit of the compact feature can be fully recognized when comparing ARIES-CS to all six stellarators[20,21,28-30] developed to date (see Fig. 13). The most recent advanced physics and technology and innovative means of radial dimension control helped reduce the major radius by more than threefold, approaching that of advanced tokamaks.

Table III

Key Nuclear Parameters for the Reference and Backup Systems

	LiPb/He/FS	**LiPb/SiC**
Peak NWL	5.3 MW/m^2	
Average NWL	2.6 MW/m^2	
Peak to average NWL	2	
Overall TBR	1.1	
Li enrichment	70%	< 90%
FW end-of-life fluence	15.7 MW/m^2	18 MW/m^2
FW/blanket lifetime	3 FPY	3.4 FPY
Shield/manifold/VV/magnet lifetime	40 FPY	
Overall energy multiplication	1.16	1.1
Δ_{min}	1.3 m	1.3 m
Δ_{max}	1.8 m	1.4 m

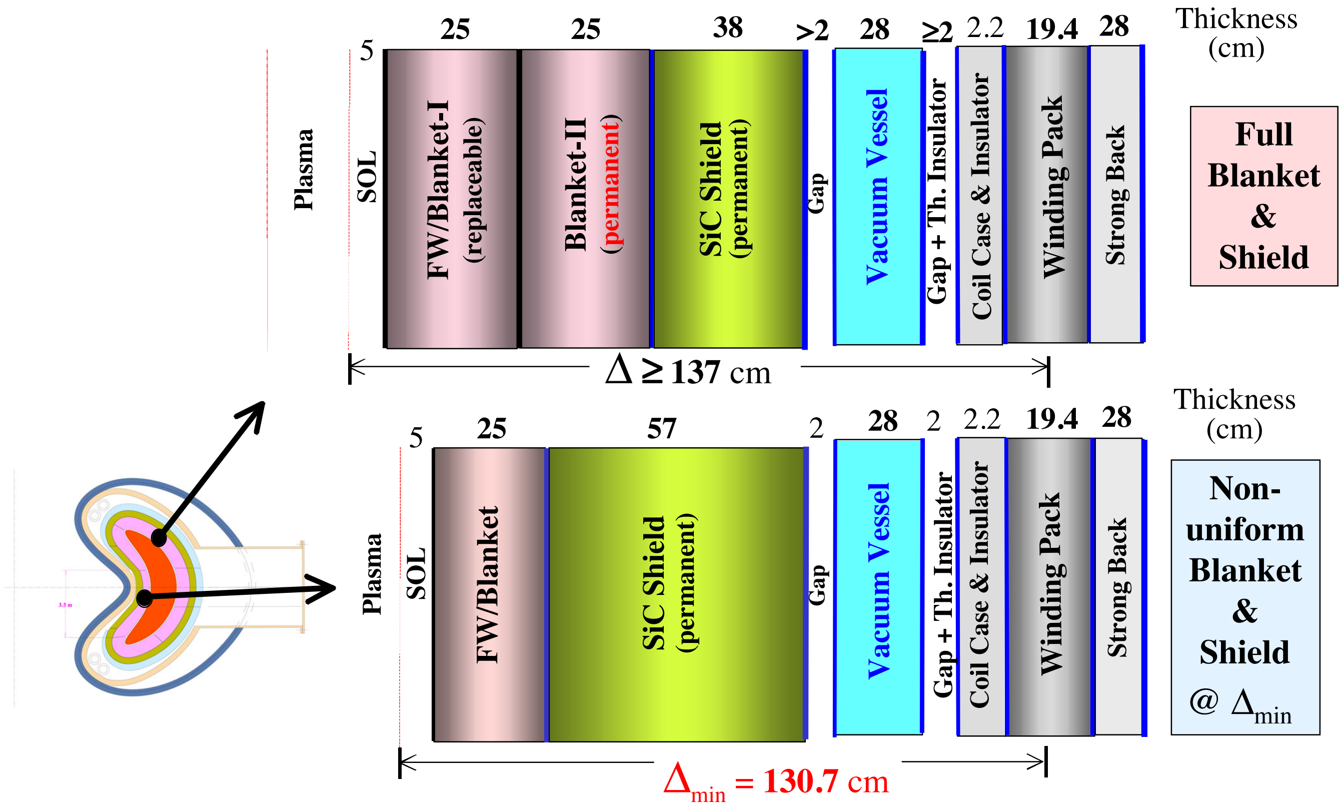

Fig. 12. Radial builds for the backup, advanced LiPb/SiC blanket designed for 4 MW/m^2 peak NWL.

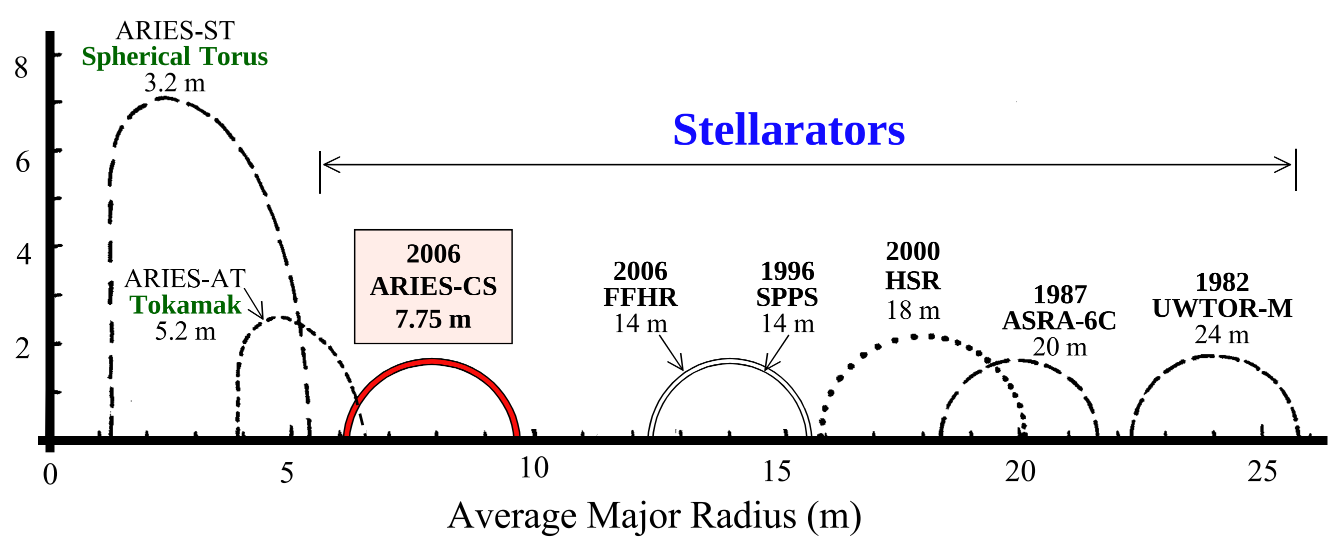

Fig. 13. Average major and minor radii of stellarator designs developed to date. Advanced tokamak and spherical torus included for comparison.

IV. FW AND BLANKET PARAMETERS

During the 3-y period of the study, several blanket/shield systems have been considered employing advanced ferritic steel (FS) structure (such as IEA MF82H) and SiC/SiC composites. The list of candidates includes four liquid breeder-based systems and one solid breeder-based system:

- Self-cooled Flibe with beryllium multiplier and advanced ODS-FS structure,
- Self-cooled LiPb with SiC/SiC composites,
- Dual-cooled LiPb (or Li) with He and FS structure, and
- He cooled Li_4SiO_4 with beryllium multiplier and FS structure.

The blanket must breed sufficient tritium for plasma operation, recover > 90% of the neutron energy, and protect the shield (dpa < 200 dpa) for the entire plant life (40 FPY). The 5-10% energy leaking into the shield must be recovered as high-grade heat to enhance the power balance. The blanket and shield help protect the welds of manifolds and VV (< 1 He appm) and all three components protect the superconducting magnets for life. Addressing the breeding issue, we had to make an educated assumption that is essential for the accuracy of the breeding level. We assumed that the penetrations and divertor plates/baffles cover 1% and 15% of the FW area, respectively. Due to the complexity of the 3-D geometry, we relied heavily on the simple 1-D poloidal cylindrical model using the average plasma minor radius to predict the overall TBR and M_n, combining 1-D estimates with blanket coverage fractions. As the design progressed, a 3-D analysis was judged essential to confirm the key nuclear parameters and to generate the neutron wall loading profile. Based on the initial assessment, the following general observations can be made:[4,26,31]

- The Flibe system always needs a beryllium or lead multiplier to meet the breeding requirement. The Flibe cools the first wall (FW), turns around and flows through the beryllium and breeding zones. The system has a coolant outlet temperature of 700 ^oC and a thermal conversion efficiency (η_{th}) of 45% and requires an advanced ODS-FS structure with an operating temperature limit of ~800 ^oC.
- This LiPb/SiC design utilizes the advanced SiC/SiC composites as the main structural material. The LiPb flows through the SiC structure at a high speed, and then flows slowly within the breeding zone. The high operational temperature of the SiC makes it possible to achieve high LiPb outlet temperature (~1100 ^oC).

The significance of the high operating temperature lies in the superior thermal conversion efficiency of the system (55-60%).

- The dual coolant option holds the potential to achieve a LiPb exit temperature ~150 degrees higher than the maximum allowable FS structure temperature to ensure high η_{th} (40-45%). Both LiPb/He/FS and Li/He/FS designs are very similar. The helium cools the FS structure while the LiPb (or Li) flows slowly in the breeding zone. Serving as a liner for the structure, a 0.5 cm thick SiC insert for the LiPb system (or AlN coating for the Li system) must be used to control the MHD effect and maintain the FS temperature below 600 ^{o}C.
- The solid breeder (SB) design requires a Be neutron multiplier to achieve tritium self-sufficiency. The proposed design[31] features multiple Li_4SiO_4 and Be layers sandwiched between cooling channels arranged parallel to the FW to efficiently remove the nuclear heating and operate within the temperature windows for Be and SB. This design can deliver electricity with η_{th} in the 40-45% range.

As is evident, each blanket concept offers advantages and drawbacks. An integrated study with guidance from the nuclear analysis and blanket design identified the preferred concept (the dual cooled LiPb/He/FS with 42% η_{th}) and a more advanced LiPb/SiC concept as a backup. The rationale for the latter is that as new developments occur, a future hope is the prospect of using SiC/SiC composites as the main structure for a high-temperature blanket (> 1000 ^{o}C), offering high thermal conversion efficiency (56%) to enhance the economics.

IV.A. Initial 1-D TBR Estimate

For each blanket, we developed three radial builds at Δ_{min}, divertor region, and nominal area everywhere else. The nominal radial build varies widely with blanket concepts (1.8 m for LiPb/He/FS and 1.4 m for LiPb/SiC). As for the blanket itself, we sized it to essentially meet the breeding requirement and protect the shield for the 40 FPY plant life. The nominal FW, breeding zone, and back wall of the LiPb/He/FS and LiPb/SiC systems are 63 and 50 cm thick, respectively. The analysis assumes a few blanket modules can be installed behind the divertor plates (20 cm FS/W/He thick, 33/4/63 by volume). The non-uniform, tapered blanket (25 cm thick at Δ_{min}) expands and joins the full blanket (see Fig. 11). Depending on the major radius, it covers 15-35% of the FW area. To estimate the overall TBR, we combined the 1-D local TBR with the coverage fraction of the three regions: nominal, non-uniform, and divertor blankets. Figure 14 shows the contours that bound the non-uniform blanket within each field period. The larger the machine, the lower the non-uniform blanket coverage, the higher the breeding. Using the coverage fraction and the 1-D TBR estimates, we examined the sensitivity of TBR to the machine size. It is customary when using 1-D models to make conservative assumptions and add a safety margin. Figure 15 shows the conservative 1-D estimate of TBR. A design with a major radius less than 7.5 m even with 90% Li enrichment cannot provide tritium self-sufficiency. This clearly demonstrates the important role the breeding requirement plays in determining the smallest major radius of compact stellarators – a feature unique to this concept.

The reference LiPb/He/FS design calls for a 7.75 m machine that meets the overall design space requirements and barely satisfies the limit on the heat load accommodation of the LiPb/He/FS blanket. The final divertor design suggests a slight change in the divertor coverage fraction (~12% of the FW area, instead of 15%). It seems likely that the 7.75 m design with 90% Li enrichment will breed more tritium than needed for plasma operation, allowing a larger breeding margin. To achieve an overall TBR of 1.1, a lower Li enrichment than 90% could be considered. However, a decisive action to adjust the enrichment could not be taken without establishing a 3-D model for the entire machine to confirm the 1-D TBR estimate. Section IV-C presents the final 3-D analysis and results.

IV.B. Heat Load to In-Vessel Components

The power deposited in the FW, blanket, shield, and divertor components will be recovered by the He and LiPb coolants as a high-grade heat. Table IV details the breakdown of the volumetric nuclear heating deposited in these in-vessel components, assuming the divertor covers 15% of the FW area. As the table indicates, most of the power (94%) goes to the FW, divertor, and blanket. The shield and manifolds carry 6% of the nuclear heating, which is significant and must be recovered to improve the power balance and enhance the economics. The small heat leakage to the VV (~ 3 MW) will be dumped as a low-grade heat. The heat load to the winding pack and intercoil structure is ~12 kW, corresponding to a LHe cryogenic load of ~5 MW_e. For a neutron power of 1884 MW (80% of the 2355 fusion power), the overall neutron energy multiplication (M_n) amounts to 1.16. The total heat deposition along with the power density that peaks at 44 W/cm^3 served as a source term for the detailed thermal analysis carried out for the ARIES-CS design.[22]

The power split between the He and LiPb coolants is an essential input to the power conversion system and to the systems code for the purpose of costing the He and LiPb heat transfer/transport system. The distribution of power including the surface heating is summarized in Table V. The 1377 MW recovered by the helium coolant includes the 111 MW transferred through the SiC insulator from the hot LiPb to the colder He.[22] About 90% of the He pumping power (183 MW_e) will be recovered by the helium coolant as a friction power. The bottom-line result is that the thermal power split between He and LiPb is 49:51.

Table IV

Nuclear Heat Load (in MW) to In-vessel Components of LiPb/He/FS System

	Full Blanket/Shield	Divertor Region	Non-uniform Blanket/Shield	Total
FW	116	--	46	162
Divertor	---	149	---	149
Blanket	1137	159	425	1729
Back wall	9	3	6	18
Shield	59	20	41	120
Manifolds	6	1	---	7
Total	1327	332	526	2185
				($\Rightarrow M_n = 1.16$)

Table V

Summary of Thermal Power Load (in MW) to Helium and LiPb Coolants of LiPb/He/FS System

	Helium	LiPb	Total
Surface heating	471	---	471
90% of He pumping power	165	---	165
FW	116	--	162
Divertor	149	---	149
Blanket	179	1550	1729
Back wall	18	---	18
Shield	120	---	120
Manifolds	2	5	7
Leakage from LiPb to He	+111	-111	0
Total	1377	1444	2821
	(49%)	(51%)	

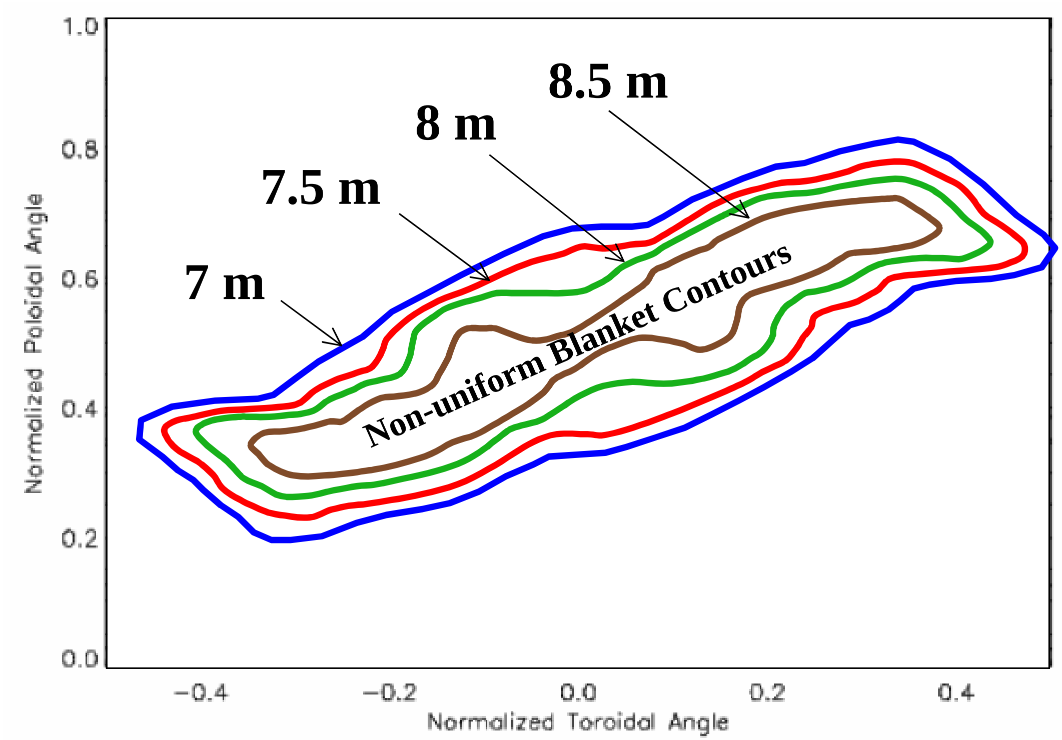

Fig. 14. Contours of non-uniform blanket covering 15-35% of the total FW area.

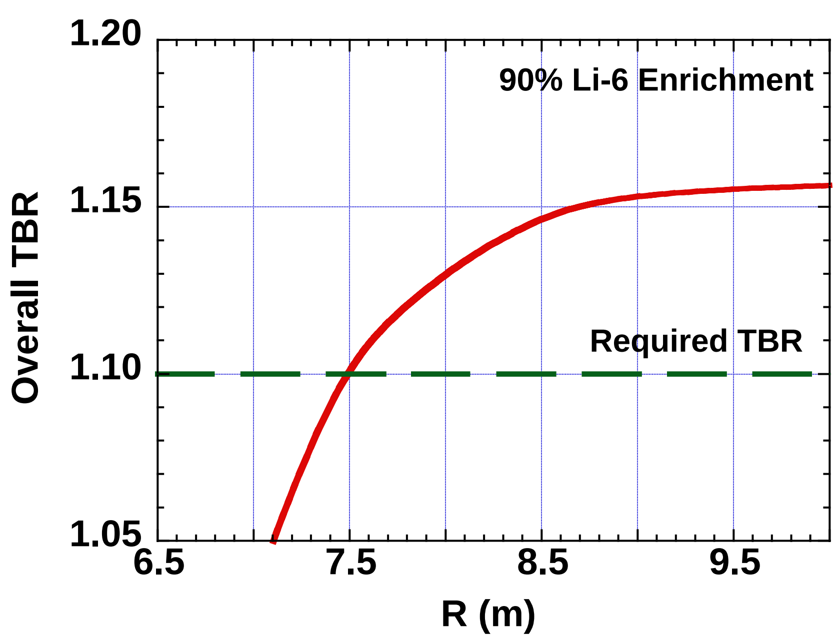

Fig. 15. 1-D estimate of TBR vs. major radius.

IV.C. Final 3-D TBR and M_n Analysis

A model of the full ARIES-CS system was developed based on a 1/6 toroidal solid model. The primary goals of this analysis were to determine the tritium breeding ratio and neutron energy multiplication for the LiPb/He/FS system in the complex ARIES-CS geometric configuration. The solid model was generated with blanket, shield, manifold, and divertors as shown in Fig. 16. A number of features were incorporated in the model to account for design elements. Since the blanket model was not constructed to distinguish between the front wall, back wall and central breeding region, a homogenized material definition was used throughout. However, this central breeding region is not of uniform thickness throughout the blanket. To accommodate this, the blanket was divided into two regions, one region with a material description consistent with the nominal blanket thickness ("uniform" region with 68% LiPb, 13.6% FS, 6% SiC, 12.4% He) and one region with a material description based on the varying blanket thickness ("non-uniform" region with 54% LiPb, 17% FS, 6% SiC, 10% B-FS, 13% He). In addition the blanket regions behind the divertors were modeled as separate regions with different homogenized mixtures (65.5% LiPb, 17.2% FS, 8% SiC, 9.3% He). To accommodate their impact on the tritium breeding ratio, the electron cyclotron heating (ECH) ducts were also included in the model as rectangular penetrations (24 x 54 cm) through the blanket, shield and manifolds at 35^{o} in each field period. Due to the complexity of the model, the vacuum vessel was not included in this analysis since its impact on the TBR and M_n is negligible.

Since periodic boundary conditions were not available for use on this MCNPX-CGM model, it was necessary to replicate the 1/6 model (~8.5 m long) with appropriate rotations to generate a full toroidal model. Axial asymmetries in the model prevented the generation of a true union of these sectors and an approximately 1 cm thick region was introduced at each boundary to alleviate this problem. Each of these regions is modeled as a void and assumed to be a small perturbation to the system. Finally, one limitation of the source function described above is that the source can only be generated in a single region. Since the model is made from 6 sectors, there are 6 different source regions. This was overcome by modeling the full toroidal system with only 1/6 of the source. Consider a component, *C*, in sector *i*. The response of this component to a full source, $R_{C_i,T}$, is the superposition of the responses from the source in each sector $R_{C_i,j}$, where j=[1,6]. However, by symmetry, the response of component C in sector i due to a source in sector j is equivalent to the response of component C in sector j due to a source in sector i: $R_{C_i,j} = R_{C_i,i}$. Therefore, $R_{C_i,T} = \frac{1}{6}\sum_j R_{C_i,j} = \frac{1}{6}\sum_j R_{C_j,i}$.

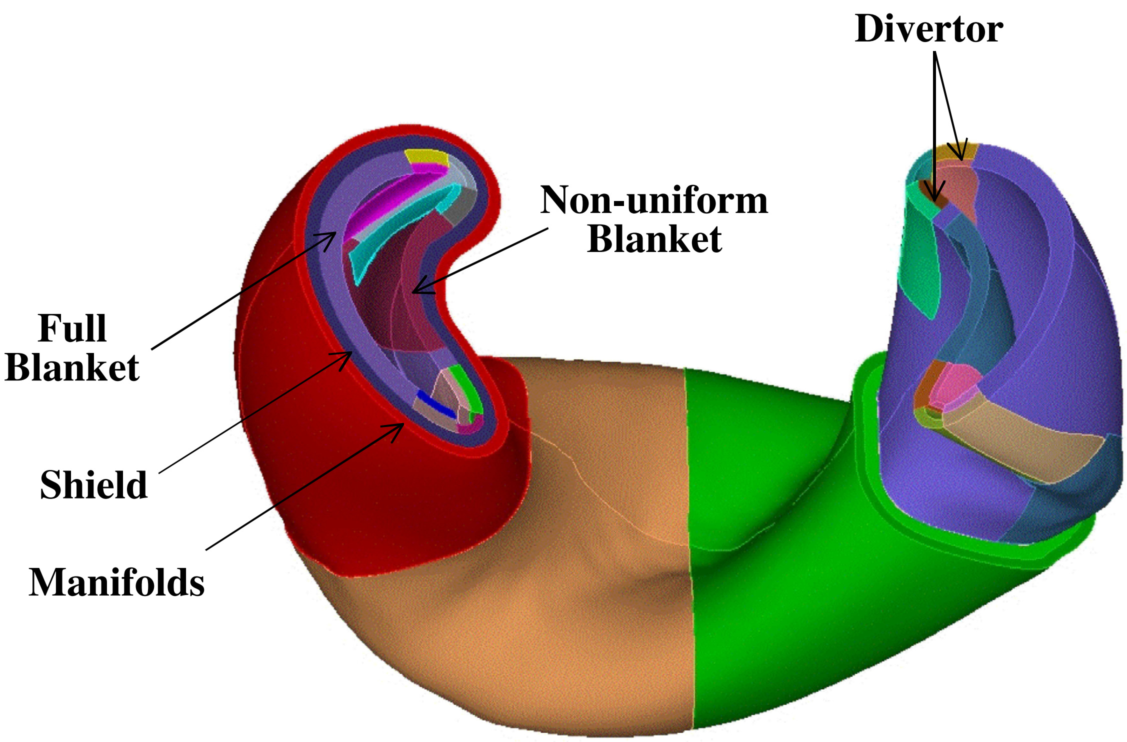

Fig. 16. Three-dimensional neutronics model of ARIES-CS.

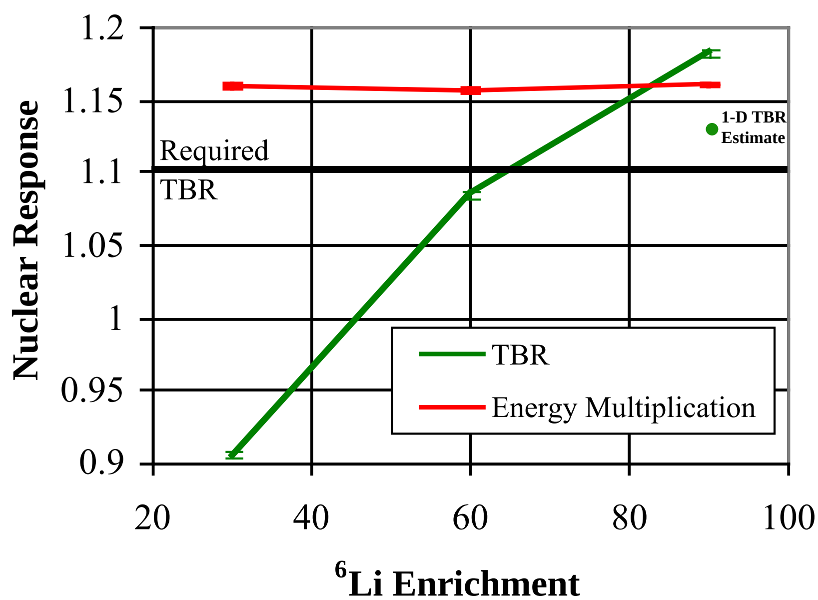

Fig. 17. Variations in TBR and M_n with ^{6}Li enrichment. Error bars indicate 1 sigma statistical errors.

Using this methodology, the results for TBR and M_n were determined for each major component and for the whole device. Figure 17 shows a summary of the variations in these integral responses as a function of the ^6Li enrichment in the blanket. The target TBR of 1.1 is indicated in the figure and suggests a ^6Li enrichment of at least 65%. Approximations introduced by the homogenization of the material for the blanket introduce some uncertainties and suggest a slightly higher enrichment of ~70%. Table VI summarizes the results for the TBR, showing the distribution of tritium breeding among the major blanket regions. In all cases, the majority (> 77%) of the tritium breeding occurs in the uniform blanket region and approximately 2.5% occurs in the blanket region behind the divertors.

The energy multiplication is seen to be independent of the ^6Li enrichment, with an approximately 16% increase in the neutron source energy occurring in the system due to neutron multiplication and exothermic nuclear reactions. Approximately half of the nuclear heating is from photons: 46%/48%/52% for ^6Li enrichments of 90%/60%/30% respectively. The distribution of the energy generation is shown in Table VII with the majority occurring in the blanket, and a significant fraction (10-12%) in the divertor and shield.

IV.D. Potential Solutions for Overbreeding and Underbreeding Blankets

A TBR of 1.1 assures tritium self-sufficiency for ARIES-CS. The 10% breeding margin accounts for the uncertainties in the cross section data (~7%), approximations in geometric model (~2%), losses during T reprocessing (~1%), and T supply for future power plants (~1%). References 11 and 32 provide a more detailed breakdown of the breeding margin. Due to the +/- nature of the uncertainties in the cross section data and other approximations, the net TBR at the beginning of plant operation may range between 1.01 and 1.2. A flexible blanket design could adjust the net TBR to 1.01 after the first blanket changeout. In case of overbreeding (net TBR > 1.01), the TBR could be decreased by lowering the enrichment below 70% or replacing a few breeding modules by shielding components. In case of underbreeding (net TBR < 1.01), an easy fix would be to increase the Li enrichment to 80 or 90%. Major changes would require thickening the breeding zones (see Fig. 18), adding beryllium to the blanket, and/or increasing the major radius above 7.75 m.

IV.E. FW/Blanket Service Lifetime

As noted earlier, ARIES-CS blanket modules were designed with replaceability as a design consideration.[8] The 198 blanket modules would be built in factories, and then shipped to the plant for installation. Failure mechanisms in the structure

Table VI
Summary of 3-D TBR Results for LiPb/He/FS System
(The 1 sigma statistical error is indicated for the total TBR in each case)

Blanket Region	^{6}Li Enrichment		
	30%	*60%*	*90%*
Uniform	0.73	0.85	0.91
Non-Uniform	0.15	0.21	0.24
Behind Divertor	0.022	0.028	0.029
Total	**0.91** (±0.18%)	**1.08** (±0.19%)	**1.18** (±0.15%)

Table VII
Summary of Energy Multiplication Results for LiPb/He/FS System
(The 1 sigma statistical error is shown for the total M_n in each case)

Component/ Region	^{6}Li Enrichment		
	30%	60%	90%
Blanket	**0.99**	**1.01**	**1.03**
Uniform	0.74	0.75	0.77
Non-uniform	0.24	0.25	0.25
Behind Divertor	0.013	0.013	0.013
Shield	**0.065**	**0.052**	**0.043**
Main Shield	0.045	0.034	0.026
Behind Divertor	0.020	0.018	0.017
Manifold	**0.0014**	**0.0014**	**0.0012**
Divertor Plates	**0.10**	**0.091**	**0.086**
ECH Duct	$\mathbf{5.7 \times 10^{-5}}$	$\mathbf{5.4 \times 10^{-5}}$	$\mathbf{4.8 \times 10^{-5}}$
TOTAL	**1.16** (±0.13%)	**1.16** (±0.14%)	**1.16** (±0.12%)

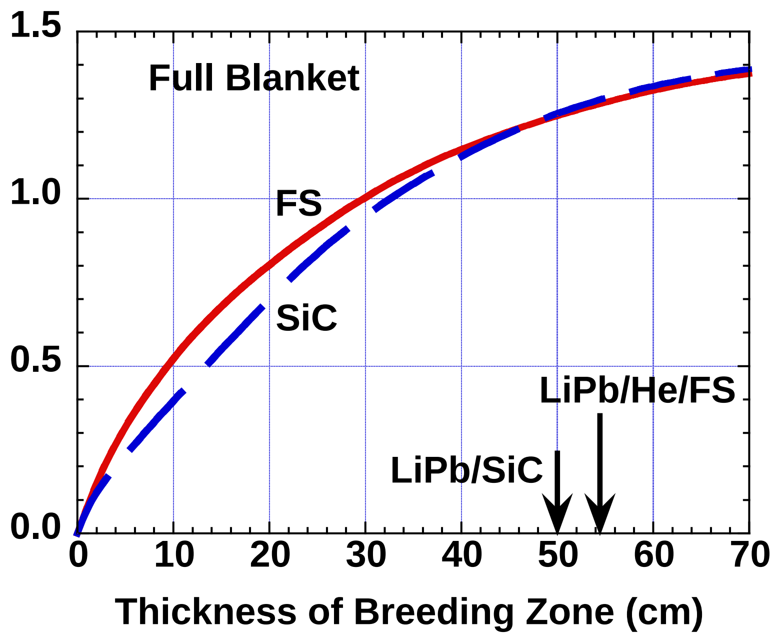

Fig. 18. TBR vs. blanket thickness.

are influenced by the atomic displacement in the case of ferritic steels and by the burnup of Si and C atoms in the case of SiC/SiC composites, ending their service lifetime. In this study, we adopted lifetime limits of 200 dpa for the FS structure and 3% burnup for the SiC structure, in concert with similar ground rules considered for advanced ARIES designs.[12,13] For a peak NWL of 5.3 MW/m^2, the FW lifetimes are 3 FPY and 3.4 FPY for the FS and SiC structures, respectively, requiring 11-13 replacements during the 40 FPY plant lifetime. Within the blanket, the SiC burnup rate drops faster than the dpa rate, calling for a thinner replaceable SiC FW/blanket (25 cm) compared to the 63 cm thick FS FW, blanket, and back wall. To help reduce the radwaste stream and the annual replacement cost, we segmented the 50 cm thick SiC blanket into two equal segments: replaceable and permanent. Even though the majority of the blanket modules are subject to NWLs less than 5.3 MW/m^2, they will all be replaced every 3-3.4 FPY. There is certainly an incremental increase in cost and radwaste volume associated with the early replacement, but this will be offset by the high gain due to the fewer maintenance processes, shorter down time, and therefore higher system availability.

V. RADIATION PROTECTION AND SHIELDING

V.A. Nominal Shield Design

We focused our shielding activity on Δ_{min} where a superior shielding performance makes a notable difference to the machine size and cost. No economic and design enhancements are gained with a high-performance, compact shield at any place, but at Δ_{min} as the nominal shielding space is not constrained elsewhere. This feature is unique to stellarators. Thus, the topic has been investigated jointly by the engineers and physicists to examine the location, size, and FW coverage of Δ_{min} and their impact on the machine parameters (major radius, field at coil, etc.), nuclear parameters (TBR, magnet protection, activation, and decay heat), and economics.

The blanket, along with the back wall, provides an important shielding function as it protects the shield for the entire plant life (40 FPY). An additional shielding criterion relates to the reweldability of the manifolds and VV. The blanket and shield must keep the neutron-induced helium at the manifolds and VV below the reweldability limit (1 appm) at any time during plant operation. All four components (blanket, shield, manifolds, and VV) help protect the superconducting magnets and externals. In our shielding analysis, we have included a safety factor of three in the results to account for the uncertainties in the computational tools and design elements.

The selection criteria for the shielding materials included several design parameters that play an essential role in the acceptability of the materials. These are the compatibility with the main structure and the constituents of other components, radiation stability, safety characteristics, and operating temperature windows. The magnet radiation limits strongly influence the compositions and size of the shielding components. Being the closest component to the magnet, the composition of the VV affects the magnet radiation damage significantly. The double-walled VV was filled with shielding materials and optimized to achieve the necessary requirements for magnet protection. Several fillers have been identified for evaluation: water, borated water, FS, and B-FS (FS with 3 wt% B). No structural role has been envisioned for the fillers. Water was considered for its superior shielding characteristics relative to other coolants such as liquid breeders and He gas. In fact, liquid breeders were excluded as the blanket and, to a lesser extent, the shield provide all the tritium needed for plasma operation.

Nb_3Sn and JK2LB (Japanese austenitic steel) have been selected as the superconductor and coil structure materials, respectively.[9] The rationale for selecting the JK2LB steel over Incoloy-908 relates to the activation characteristics of the two candidate alloys, as highlighted in Section VII and detailed in Ref. 25. The maximum radiation damage to the winding pack is limited by the 10^{19} n/cm^2 fast neutron fluence to the Nb_3Sn superconductor, dose to the insulator (10^{11} rads), and displacement of atoms for the copper stabilizer ($6x10^{-3}$ dpa). The peak nuclear heating limitation, determined by the refrigeration requirement, is 2 mW/cm^3 for the low-temperature 4 K magnet.

The proposed insulation for ARIES-CS is an inorganic tape impregnated with a ceramic binder applied to the tape prior to application to the cable. Several types of tapes have been considered including S2-glass tape that has been desized. The ceramic-based tape is wrapped around the conductor during the winding process and prior to the heat treatment using an inorganic clay-glass insulator. The lack of organic materials reduces the sensitivity of the proposed insulation to radiation damage. Inorganic insulators have a typical fluence limit on the order of 10^{11} rads (10^9 G).[9] The actual composition of the ceramic-based inorganic insulator is not available – a proprietary property of an European manufacturing company. Instead, the composition of the glass-fiber-filled polyimide has been used throughout the shielding analysis.

Our results show that the fast neutron fluence to the Nb_3Sn superconductor and peak nuclear heating are the predominant radiation limits for the magnet. The strong dependence of fluence and heating on the choice of the VV fillers is displayed in Fig. 19 for the LiPb/He/FS concept, showing the impact of the tradeoff between water and B-FS filler. The water content could range from 30 to 70%, by volume. We selected 65% water content to minimize the mass of the VV and solid radwaste without exceeding the heating and fluence limits. Sandwiched between 3 cm thick face sheets, the central part of the VV consists of 5% FS ribs (dictated by the structural requirement), 65% water, and 30% borated FS filler, by volume. Table VIII summarizes the peak radiation damage at the three distinct regions of ARIES-CS: full blanket, non-uniform blanket, and divertor. The results reflect a safety factor of three that accounts for the uncertainties in the cross section data, approximations in the 1-D model, and presence of the assembly gaps between adjacent modules. In other words, the reported results are three times higher than the computed values. The analysis assumes perfect shield with no penetrations. Admittedly, neutrons streaming through the helium supply pipes will enhance the damage, but hopefully it will not exceed the limit. Means to alleviate the streaming problems have been investigated as will be discussed shortly in Section V.C.

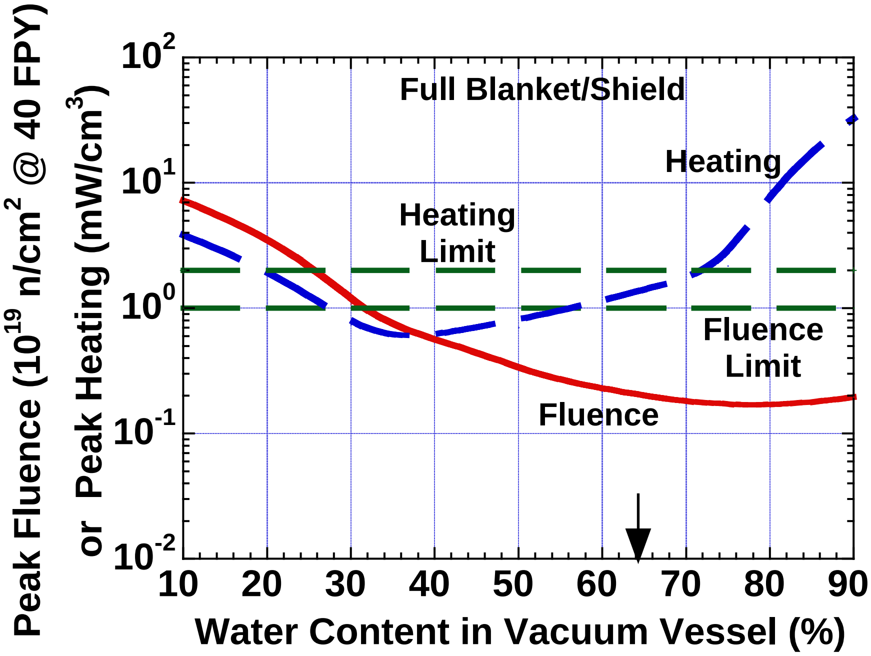

Fig. 19. Sensitivity of peak radiation effects at magnet to VV composition, trading B-FS for water.

Table VIII

Peak Radiation Damage to ARIES-CS Components

	Full Blanket/Shield	Non-uniform Blanket/Shield	Divertor Region	Radiation Limits
Peak neutron wall loading (MW/m^2)	5.3	3.3	2.7	
dpa at shield (dpa @ 40 FPY)	200	160	135	200
He production at manifolds (He appm @ 40 FPY)	1	---	1	1
He production at VV (He appm @ 40 FPY)	0.2	0.5	0.2	1
Magnet:				
Fast neutron fluence (10^{19} n/cm^2 @ 40 FPY)	0.2	0.3	0.2	1
Nuclear heating (mW/cm^3)	1.4	0.3	0.9	2
Dose to insulator (10^{10} rads)	2.4	0.7	1.5	10
dpa at Cu stabilizer (10^{-3} dpa @ 40 FPY)	1.1	2.2	1	6

We developed a high-performance, compact radial build for the critical area surrounding Δ_{min} that can withstand up to 4 MW/m^2 peak NWL. The main idea is to use a reduced size blanket with more efficient shielding materials at local spots around Δ_{min} and deploy the nominal blanket elsewhere. For the reference configuration, Δ_{min} occurs at four locations per field period and the transition region between Δ_{min} and the full nominal blanket covers ~24% of the FW area. Looking beyond conventional materials (such as steel, water, and borides), tungsten and its compounds possess superior shielding performance. Tungsten carbide, in particular, offers the most compact radial build when used in the shield, replacing the B-FS filler. Costing roughly the same as the steel filler, the WC cost difference is not prohibitive for such limited space. Figure 10 displays the LiPb/He/FS radial builds that meet the design requirements. Components with poor shield performance, such as the manifolds, have been avoided at Δ_{min}. The compact blanket/shield helps reduce the radial standoff at Δ_{min} by 50 cm, which is significant, while maintaining the radiation level below the design limit (refer to Table VIII). Considering the positive impact on the overall machine and economics,[7] it pays to incorporate the compact radial build at Δ_{min}. A challenging task would be the heat removal mechanism and the integration of the non-uniform blanket/shield with the surroundings.[33] Blanket and shield with variable thicknesses have been envisioned for the transition region as demonstrated in Fig. 11.

V.B. Bioshield

Surrounding the magnet is the 5 cm thick 304-SS cryostat, followed by the 2 m thick steel-reinforced concrete bioshield (85% concrete, 10% mild steel structure, and 5% He coolant). To size the bioshield, we took advantage of the inter-coil structure between the magnet winding packs. Along with the in-vessel components, the 15-30 cm thick inter-coil structure provides a shielding function that helps reduce the bioshield dimension. The 2 m thick bioshield limits the biological dose during operation to 0.25 mrem/h (see Fig. 20). This operational dose is consistent with the U.S. guidelines for the protection of workers and public and reflects a 10-fold reduction in the absolute limit of 2.5 mrem/h in order to keep the dose as low as reasonably achievable. The need for a sufficient space outside the magnet to conduct the maintenance operation mandates the bioshield to be placed at a radius of 13 m or more. The dose inside the bioshield is quite high even after shutdown, meaning all ARIES-CS components should be maintained remotely, with no personnel access into the hall surrounding the magnets.

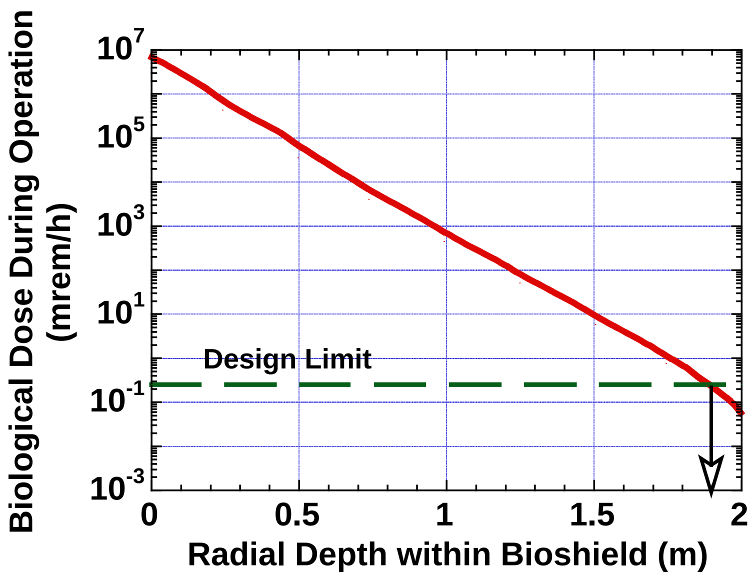

Fig. 20. Decrease of operational dose rate with bioshield thickness.

V.C. Streaming Issues

The radiation levels reported so far pertain to a perfect configuration without penetrations. Penetrations are necessary for vacuum pumping, coolant supply lines, plasma control, and maintenance ports. Such penetrations jeopardize the effectiveness of the shield as neutrons streaming through these penetrations enhance the damage at the shield, manifolds, VV, and magnet. Helium-cooled systems in particular raise a specific concern as designing penetration shields for the He access tubes/pipes represent a challenging problem. Seven types of penetration have been identified for the reference LiPb/He/FS design:

- 198 He tubes for blanket (32 cm ID)
- 24 Divertor He access pipes (30-60 cm ID)
- 30 Divertor pumping ducts (42 x 120 cm each)
- 12 Large pumping ducts (1 x 1.25 m each)
- 3 ECH ducts (24 x 54 cm each).
- 6 main He pipes connecting HX to blanket and shield (72 cm ID each)
- 6 main He pipes connecting HX to divertor (70 cm ID each)
- 4 access holes (3 cm diameter) for each blanket module.

To improve the prospects for ARIES-CS with reduced neutron streaming, we developed a list of practical solutions that could be selectively applied to each penetration:

- Local shield behind penetrations
- He tube axis oriented toward lower neutron source
- Penetration shield surrounding ducts
- Replaceable shield close to penetrations
- Avoid rewelding VV and manifolds close to penetrations
- Several bends along penetration lines.

Two- and three-dimensional analyses need to be performed to address the streaming issues and concerns. However, the definition of several penetrations came too late in the design process, suggesting a qualitative assessment for some penetrations. For instance:

- The large penetrations for ECH and He supply lines should be surrounded with 0.5-1 m thick penetration shield to protect the surroundings. The ECH hardware is embedded at the front of the blanket in an equatorial port located toroidally at ϕ= 35°. A few 90° bends along the deep penetration line help attenuate the streaming neutrons.
- Three or more bends are recommended for the vacuum pumping ducts located between the inboard and outboard divertor plates. A 50 cm thick local shield behind each duct helps protect the magnet against streaming radiation.
- The blanket access holes raise a streaming concern as the 3 cm diameter, 50 cm deep holes provide a clear path for the 14 MeV source neutrons to reach the shield. Long nuts (30-50 cm) screwed in from the plasma side are necessary to protect the four bolds located at the back of each blanket module. The holes occupy a small fraction of the blanket (< 1%) and will have insignificant impact on TBR.
- There is a close fitting shielding plug inserted into the maintenance ports during operation. These shielding components will be neutronically equivalent to the VV and intercoil structure that are missing in the port region.

More serious streaming issues related to the blanket He access tubes and divertor He access pipes were investigated in detail using 2-D and 3-D DANTSYS,[15] MCNPX,[14] and Attila[34] codes, as briefly discussed below. Note that these particular streaming problems are unique to the dual-cooled LiPb/He/FS reference design, inapplicable to the LiPb/SiC backup system. Of specific interest are the impacts of radiation streaming on the dpa, He production, and nuclear heating rates at the surrounding components (blanket, shield, manifolds, VV, and magnet). If the damage level in the structure is too high, these components will have to be replaced in order to maintain the integrity of the machine. For example, the dpa and He production levels at the shield and manifolds/VV should not exceed 200 dpa and 1 appm, respectively, at any time during operation. Also, the neutron-induced swelling at the outer screws that adjust the divertor plates (see Fig. 21) should be minimal.

V.C.1 Streaming Through Blanket He Access Tubes: The aim of this study is to estimate the radiation damage at the manifolds, VV, and magnet due to neutron streaming through the 32 cm diameter He tubes that supply the He from the manifolds to the blanket modules. One of the 198 tubes is shown schematically in Fig. 11 for the non-uniform blanket module. The results of the 2-D model indicate a high damage at the manifolds, exceeding the 1 appm reweldability limit at 40 FPY. To protect the manifolds, the analysis suggests increasing the nominal shield thickness to 32 cm and orienting the tubes away from the high neutron source that peaks at the plasma center. In addition, an innovative idea suggests protecting the welds further with a removable 10 cm thick WC shielding ring.[23] In this case, the welds will not be in a direct line of sight with the streaming neutrons, but rather embedded in the manifold structure, away from the tube surface.

The damage profile at the VV and magnet indicates the streaming results in hot spots peaking behind the tube centerline and the damage exceeds the limit by more than an order of magnitude. To protect the VV and magnet, approximately 25 cm thick local shield should be placed behind each tube, as illustrated in Fig. 11. The toroidal and poloidal extents of these local shields need to exceed the 32 cm diameter of the tube to adequately protect the VV and magnet against streaming radiation.

V.C.2 Streaming Through Divertor He Access Pipes: A set of four pipes is required to supply the He coolant to each divertor system. The pipe begins behind the divertor and extends outward through the blanket, shield, manifolds, VV, and coil structure. Our preliminary 2-D analysis for a 40 cm diameter pipe indicates that the peaking in damage near the pipe surface is more pronounced at the magnet than at the shield. Furthermore, the damage due to streaming increases by 2-10 fold, depending on the response function and component. Moreover, the neutron flux behind the pipe outside the magnet increases by four orders of magnitude. These results mandate redesigning the pipe with internal shielding plugs and bends to control the streaming radiation. Figure 21 displays a design approach that would be maintainable while offering several attractive features that alleviate the streaming problem. The 3-D analysis for the four pipes is ongoing at this writing and the results will be published at a later date.[35] The tools utilized to analyze this 3-D problem are the Attila deterministic code[34] and MCNPX Monte Carlo code.[14] Both codes import a CAD model of the divertor and four pipes, eliminating modeling errors and allowing faster design iterations, if needed.

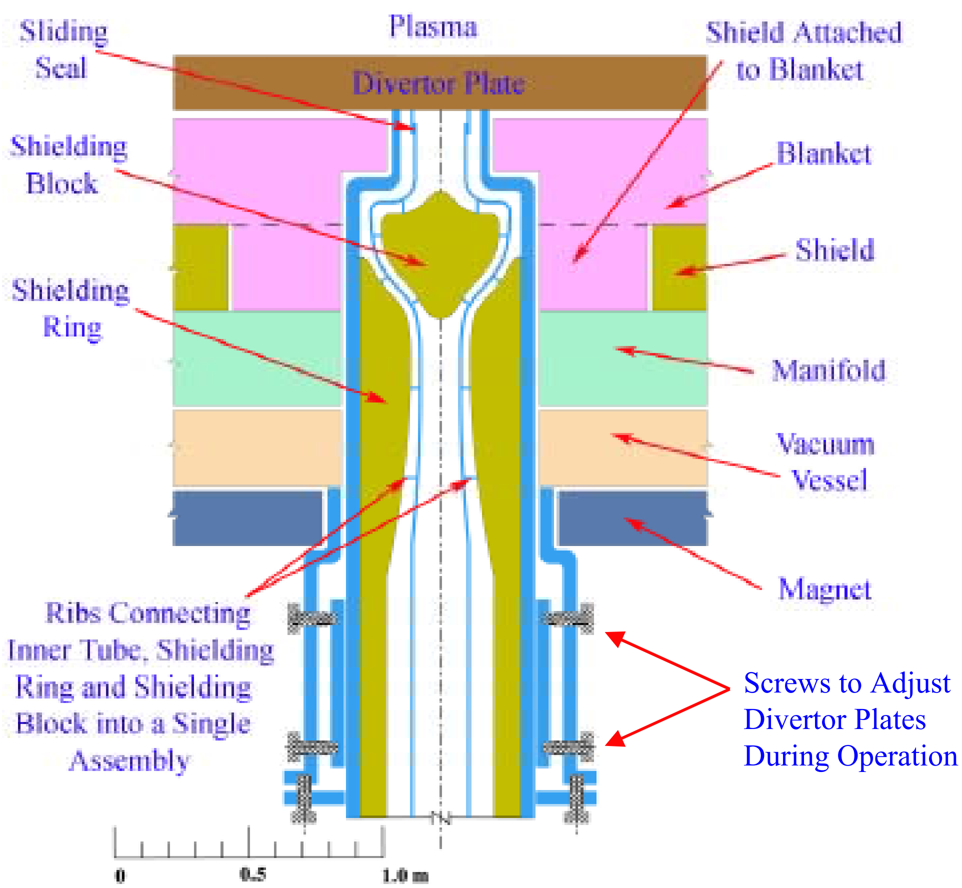

Fig. 21. Helium access pipe for ARIES-CS divertor system.

VI. COMPARISON BETWEEN LiPb/He/FS AND LiPb/SiC SYSTEMS

There are two primary aspects for this comparison: nuclear performance and economics. The first aspect relates to the radial build, breeding capacity, shielding performance, and activation level. The second aspect must also be considered to assess the economic impact of introducing the helium coolant to the LiPb/FS system in order to solve the MHD problem. Other aspects outside the scope of this assessment, such as the thermal and mechanical performances and technological readiness, could be important issues, but will not be addressed here.

The nominal radial build varies widely with up to 42 cm difference, as Figs. 10 and 12 indicate. This translates into more materials and sizable components for the LiPb/He/FS system. In addition, the He and LiPb manifolds that surround the shield represents another hefty component. Sizable helium tubes and pipes connecting the manifolds to the blanket, shield, and divertor raise neutron streaming concerns and require numerous patches of local shields behind the pipes to protect the VV and magnet. As far as breeding is concerned, both systems satisfy the breeding requirement with ~50 cm thick blanket. The SiC system offers a slightly longer FW/blanket lifetime, slightly lower energy multiplication, remarkably higher thermal efficiency, but more expensive structure (510 $/kg for SiC/SiC composites vs. 103 $/kg for FS). Cost credits are anticipated for the SiC system due to the absence of He pumping power (~180 MW_e) and He heat transfer/transport loop. The very low activation of SiC translates into more attractive safety features expressed in the level of safety assurance (LSA=1 for SiC system and LSA=2 for FS system; the lower the LSA, the lower the cost). An integrated economic analysis[7] assessed self-consistently the impact of all these features and parameters on the overall cost of ARIES-CS and Table IX shows the evaluation of the two systems. Overall, the cost of electricity (COE) metric used to evaluate all ARIES concepts indicates a 20-25% better economic performance for the SiC system.[7] In other words, the He-cooled FS system increments the COE by ~18 mills/kWh.

Table IX

Comparison Between Reference and Backup Systems

	LiPb/He/FS	**LiPb/SiC**
Overall TBR	1.1	1.1
FW/blanket lifetime	3 FPY	3.4 FPY
Overall energy multiplication	1.16	1.1
η_{th}	42%	56%
Structure unit cost	103 $/kg	510 $/kg
Blanket/divertor/shield/manifolds cost*	$288M	$282M
Cost* of heat transfer/transport system	$475M	$175M
Pumping power	183 MW_e	---
LSA factor	2	1
COE*	78 mills/kWh	60.2 mills/kWh

* in 2004 $.

VII. HIGHLIGHTS OF ACTIVATION AND WASTE MANAGEMENT ASSESSMENTS

As the safety assessment frequently requires knowledge of the activation parameters, we estimated the highest possible activity, decay heat, and radwaste level on the 100 y timescale after shutdown. As a source term, the activity has been used to generate the decay heat for the loss of coolant/flow accident (LOCA and LOFA) analysis[23,24] and to evaluate the radiological hazards of the individual components.[25] For all components except the divertor system, the decay heat is manageable, resulting in a LOCA/LOFA temperature below the 740 ^oC reusability limit of FS.[23] The W of the divertor generates high decay heat and the LOCA/LOFA temperature exceeds 800 ^oC, necessitating replacement of the divertor system following an accident or installing an active heat removal system operating for the first 24 hours.

Since the inception of the ARIES project, we focused our attention on the disposal of all active materials in geological repositories. To classify the waste, we evaluated the waste disposal rating for a fully compacted waste using the most conservative waste disposal limits developed in the U.S. In general, ARIES plants generate only low-level waste (Class A or C) that requires near-surface, shallow-land burial according to the U.S. waste classification. The recent introduction of the clearance category for slightly radioactive materials and the development of radiation-hardened remote handling equipment opened the possibility to recycle and clear the majority of the ARIES-CS radwaste. Scenarios for fusion radwaste management now include disposal in geological repositories, recycling and reuse within the nuclear industry if technically and economically feasible, and clearance or release to the commercial market if the materials contain traces of radioactivity. There is a growing international effort in support of this new trend to essentially avoid the repository disposal and eliminate the long-term radwaste burden on future generations. We applied the disposal, recycling, and clearance scenarios to all ARIES-CS components. The recycling and clearance options appeared technically attractive and judged necessary to control the ARIES-CS radwaste stream. Noteworthy, this activation assessment limited the material choices for one of ARIES-CS components. It provided a definitive answer to "what is the best structural material for ARIES-CS magnet: JK2LB or Incoloy-908?" The superior recycling and clearance characteristics of the JK2LB Japanese steel provided a strong incentive to use it as the reference magnet structure. For more detailed discussion, the reader is directed to the ARIES-CS safety paper in this issue.[25]

Over the past three decades, the radwaste volume aspect of fusion continued to be of a concern. As such, the ARIES project has been committed to the achievable goal of radwaste minimization by design. Figure 22 displays the breakdown of ARIES-CS radwaste. The focus on compact devices with radwaste reduction mechanisms (such as well-optimized components) contributed most significantly to the 3-fold reduction in ARIES-CS total radwaste volume compared to previous stellarators developed prior to 1990.[28,29] Figure 23 demonstrates this impressive trend and illustrates the 30% reduction in ARIES-CS volume achieved even during the 3 year timeframe of the study. In fact, recycling and clearance can be regarded as a more effective means to diminish the radwaste stream. The reason is that clearable materials will not be categorized as waste and the majority of the remaining non-clearable materials can potentially be recycled indefinitely and therefore, will not be assigned for geological disposal.

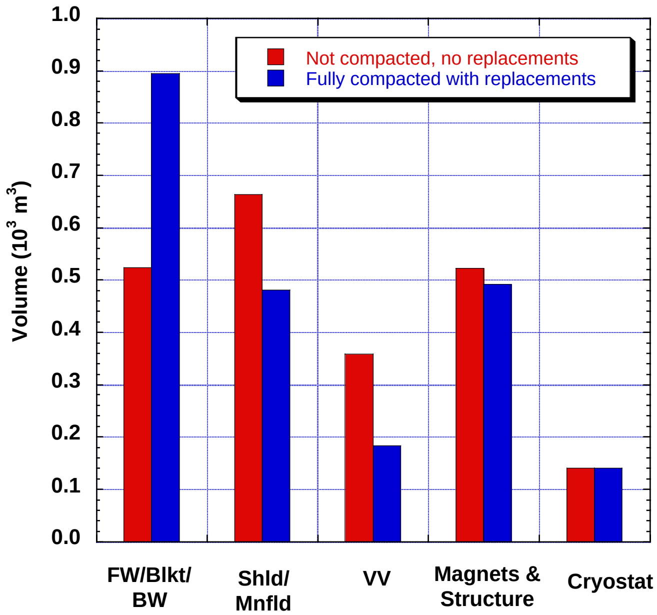

Fig. 22. Breakdown of ARIES-CS radwaste volumes.

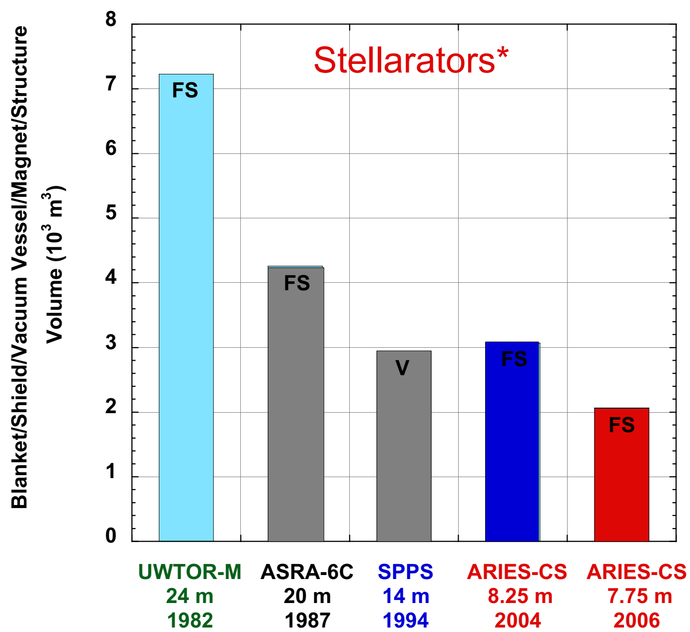

Fig. 23. Evolution of in-vessel components and magnet volumes for U.S. stellarators developed over the past 30 years (actual volumes, no compactness, no replacements).

VIII. CONCLUSIONS

The three unique aspects of ARIES-CS, namely advanced physics, advanced technology, and advanced manufacturing techniques, driven by the guiding principle of compactness, have resulted in as economically competitive stellarator power plant. A number of challenging engineering issues have been addressed in order to deliver a credible design. Among other factors, these issues stem from the compactness and complexity of the machine. Serious efforts have been made to address the nuclear-related issues in particular, by adjusting the radial standoff to accommodate the constrained areas where the magnet moves close to the plasma, developing a new CAD/MCNP tool to model, for the first time ever, such a complex geometry for 3-D nuclear analyses, and establishing a framework for handling the radioactive materials and minimizing the radwaste stream.

The first and foremost effort has been on defining the components of the minimum plasma-coil space which is the most influential engineering element that greatly impacts stellarators' overall size and cost. Through rigorous nuclear analysis, we demonstrated that:

- The novel approach developed for Δ_{min} helps reduce the radial standoff, major radius, and COE by 25-30%, which is significant. Equally important is the consequence of the substantial reduction in ARIES-CS radwaste volume compared to previous stellarator designs.
- The tritium breeding plays an important role in determining the minimum major radius of compact stellarators – a unique feature to compact stellarators.
- The reference blanket and shield design satisfies the design requirements, breeding sufficient tritium and protecting vital components with adequate margin. The FW/blanket and divertor need frequent replacement every 3 FPY while the shield, manifolds, VV, and magnet are life-of-plant components.
- Exact modeling of any stellarator for 3-D nuclear assessment would not be possible without the CAD/MCNP coupling approach. Its development proved to be a must requirement to accurately generate the NWL profile and confirm the overall nuclear parameters (TBR and M_n)
- Streaming through helium supply tubes/pipes may cause serious damage problems unless penetrations are properly designed to attenuate streaming radiation.

- Attention should be paid to radwaste management issues. A recycling/clearance strategy to control stellarators' waste stream must be developed in concert with present U.S. regulation and growing international effort in support of this new strategy.

With technologies shifting constantly for advantages as new developments occur, the prospect of using SiC/SiC composites as the main structure offers high operating temperature, high thermal conversion efficiency, and salient safety features – all are potential enhancers for the economic performance of the LiPb/SiC backup system. The absence of the helium coolant and consequences related to streaming problems and use of numerous local shields around the He access pipes represent an additional advantage for the LiPb/SiC system.

ACKNOWLEDGMENT

This work was performed under the auspices of the U.S. Department of Energy (contract # DE-FG02-98ER 54462).

REFERENCES

1. The NCSX Project: http://www.pppl.gov/ncsx/.
2. F. NAJMABADI, “Overview of ARIES-CS Power Plant Study,” this issue.
3. L.P. KU, P.R. GARABEDIAN, J. LYON, et al, “Physics Design for ARIES-CS,” this issue.
4. L. EL-GUEBALY, R. RAFFRAY, S. MALANG, J. LYON, and L.P. KU, “Benefits of Radial Build Minimization and Requirements Imposed on ARIES-CS Stellarator Design,” *Fusion Science & Technology*, **47**, No. 3, 432-439 (2005).
5. M. WANG, D. HENDERSON, T. TAUTGES, L. EL-GUEBALY, and X. WANG, “Three -Dimensional Modeling of Complex Fusion Devices Using CAD-MCNP Interface,” *Fusion Science & Technology*, **47**, No. 4, 1079-1083 (2005).
6. L. EL-GUEBALY, P. WILSON, and D. PAIGE, “Initial Activation Assessment of ARIES Compact Stellarator Power Plant,” *Fusion Science & Technology*, **47**, No. 3, 440-444 (2005).
7. J. LYON, L.P. KU, L. EL-GUEBALY, and L. BROMBERG, “Systems Studies and Optimization of the ARIES-CS Power Plant,” this issue.
8. L. WAGANER, R. J. PEIPERT-Jr, X. WANG, and S. MALANG, “ARIES-CS Maintenance System Definition and Analysis,” this issue.
9. X. WANG, A. RAFFRAY, L. BROMBERG et al., “ARIES-CS Magnet Conductor and Structure Evaluation,” this issue.
10. F. NAJMABADI, M. S. TILLACK, R.L. MILLER et al., “The Starlite Study: Assessment of Options for Tokamak Power Plants,” University of California-San Diego, UCSD-ENG-005 (1997).
11. L.A. EL-GUEBALY, "Overview of ARIES-RS Neutronics and Radiation Shielding: Key Issues and Main Conclusions," *Fusion Engineering and Design*, **38**, 139-158 (1997).
12. L.A. EL-GUEBALY, “ARIES-ST Nuclear Analysis and Shield Design,” *Fusion Engineering and Design*, **65**, 263-284 (2003).
13. L.A. EL-GUEBALY, “Nuclear Performance Assessment of ARIES-AT,” *Fusion Engineering and Design*, **80**, 99-110 (Jan 2006).
14. X-5 Monte Carlo Team, “MCNP-A General Monte Carlo N-Particle Transport Code, Version 5-Volume II: Users Guide,” LA-CP-03-0245, Los Alamos National Laboratory (April 2003).

15. R. ALCOUFFE et al., "DANTSYS: A Diffusion Accelerated Neutral Particle Transport Code System," Los Alamos National Laboratory Report, LA-12969-M (1995).
16. The FENDL-2 175 neutron 42-gamma group coupled cross-section library is available at: http://www.iaea.org/.
17. P. WILSON and D. HENDERSON, "ALARA: Analytic and Laplacian Adaptive Radioactivity Analysis Code Technical Manual," University of Wisconsin Fusion Technology Institute, UWFDM-1070 (January 1998). Available at: http://fti.neep.wisc.edu/pdf/fdm1070.pdf.
18. T.J. TAUTGES, M.K. WANG, and D.L. HENDERSON, "CAD-Based Monte Carlo Transport Using MCNPX and CGM," Transactions of 2004 ANS Winter Meeting, Washington, DC, Nov. 14-18, 2004.
19. T.D. BLACKER et al., "CUBIT mesh generation environment, Vol. 1: User's manual," SAND94-1100, Sandia National Laboratories, Albuquerque, New Mexico, May 1994. Available at: http://endo.sandia.gov/cubit/release/doc-public/Cubit_UG-4.0.pdf.
20. R. MILLER and the SPPS Team, "The Stellarator Power Plant Study," University of California San Diego Report UCSD-ENG-004 (1996).
21. C.D. BEIDLER, E. HARMEYER, F. HERRNEGGER et al., "Recent Developments in Helias Reactor Studies," Proceedings of 13th International Stellarator Workshop, Canberra, Australia, Feb. 25-March 1 (2002).
22. A. RAFFRAY, L. EL-GUEBALY, T. IHLI, S. MALANG, X. WANG, and B. MERRILL, "Engineering Design and Analysis of the ARIES-CS Power Plant," this issue.
23. C. MARTIN and L. EL-GUEBALY, "Modeling and Analysis of Loss of Coolant and Loss of Flow Accidents in the ARIES-CS Fusion Power Plant," University of Wisconsin Fusion Technology Institute Report, UWFDM-1302 (Feb. 2007). Available at: http://fti.neep.wisc.edu/pdf/fdm1321.pdf.
24. C. MARTIN and L. EL-GUEBALY, "ARIES-CS Loss of Coolant and Loss of Flow Accident Analyses," to be published in *Fusion Science & Technology*.
25. B. MERRILL, L. EL-GUEBALY, C. MARTIN et al., "Safety Assessment of the ARIES Compact Stellarator Design," this issue.
26. Available at: http://fti.neep.wisc.edu/aries-cs/builds/build.html.
27. R. RAFFRAY, L. EL-GUEBALY, S. MALANG, and X. WANG, "Attractive Design Approaches for a Compact Stellarator Power Plant," *Fusion Science & Technology*, **47**, No. 3, 422-431 (2005).

28. B. BADGER et al., "UWTOR-M, A Conceptual Modular Stellarator Power Reactor," University of Wisconsin Fusion Engineering Program Report UWFDM-550 (1982). Available at http://fti.neep.wisc.edu/pdf/fdm550.pdf.

29. G. BÖHME, L.A. EL-GUEBALY, G.A. EMMERT et al., "Studies of a Modular Advanced Stellarator Reactor ASRA6C," Fusion Power Associates Report FPA-87-2 (1987). Available at: http://fti.neep.wisc.edu/pdf/fpa87-2.pdf.

30. A. SAGARA, O. MITARAI, S.IMAGAWA et al., "Conceptual Design Activities and Key Issues on LHD-Type Reactor FFHR," *Fusion Engineering and Design*, **81**, 2703-2712 (2006).

31. R. RAFFRAY, S. MALANG, L. EL-GUEBALY, and X. WANG, "Ceramic Breeder Blanket for ARIES-CS," *Fusion Science & Technology*, **48**, No. 3, 1068 (2005).

32. M.E. SAWAN and M.A. ABDOU, "Physics and Technology Conditions for Attaining Tritium Self-sufficiency for the DT Fuel Cycle," *Fusion Engineering and Design*, **81**, 1131-1144 (2006).

33. X. WANG, S. MALANG, L. EL-GUEBALY, and R. RAFFRAY, "Integration of the Modular Dual Coolant Pb-17Li Blanket Concept in the ARIES-CS Power Plant," to be published in *Fusion Science & Technology*.

34. ATTILA Radiation Transport Software by Transpire Inc (2006). Information available at: http://www.transpireinc.com/.

35. A. IBRAHIM, D.L. HENDERSON, L. EL-GUEBALY, and P.P.H. WILSON, " Analysis of Radiation Streaming Through ARIES-CS He Access Pipes using the Attila and DAG-MCNPX Three Dimensional Neutronics Codes," to be published.